energies

MDPI

Article

# Investigating the Plasma-Assisted and Thermal Catalytic Dry Methane Reforming for Syngas Production: Process Design, Simulation and Evaluation

**Evangelos Delikonstantis, Marco Scapinello and Georgios D. Stefanidis ***

Process Engineering for Sustainable Systems (ProcESS), Department of Chemical Engineering KU Leuven, Celestijnenlaan 200F, 3001 Leuven, Belgium; evangelos.delikonstantis@kuleuven.be (E.D.); marco.scapinello@kuleuven.be (M.S.)

* Correspondence: georgios.stefanidis@cit.kuleuven.be; Tel.: +32-1632-1007

Received: 4 August 2017; Accepted: 14 September 2017; Published: 18 September 2017

**Abstract:** The growing surplus of green electricity generated by renewable energy technologies has fueled research towards chemical industry electrification. By adapting power-to-chemical concepts, such as plasma-assisted processes, cheap resources could be converted into fuels and base chemicals. However, the feasibility of those electrified processes at large scale has not been investigated yet. Thus, the current work strives to compare, for first time in the literature, plasma-assisted production of syngas, from $CH_4$ and $CO_2$ (dry methane reforming), with thermal catalytic dry methane reforming. Specifically, both processes are conceptually designed to deliver syngas suitable for methanol synthesis ($H_2/CO \geq 2$ in mole). The processes are simulated in the Aspen Plus process simulator where different process steps are investigated. Heat integration and equipment cost estimation are performed for the most promising process flow diagrams. Collectively, plasma-assisted dry methane reforming integrated with combined steam/$CO_2$ methane reforming is an effective way to deliver syngas for methanol production. It is more sustainable than combined thermal catalytic dry methane reforming with steam methane reforming, which has also been proposed for syngas production of $H_2/CO \geq 2$; in the former process, 40% more $CO_2$ is captured, while 38% less $H_2O$ is consumed per mol of syngas. Furthermore, the plasma-assisted process is less complex than the thermal catalytic one; it requires higher amount of utilities, but comparable capital investment.

**Keywords:** dry methane reforming; plasma-assisted reforming; process modeling; energy efficiency; process evaluation

## 1. Introduction

Fossil feedstocks can be converted into added value products in a two-step process, known as Fischer-Tropsch (FT) synthesis process. In the first step, syngas, a mixture of $H_2$ and CO, is formed. In the second step, syngas is converted into synthetic fuels and chemicals, according to the global reaction:

$$(2n + 1)H_2 + nCO \rightarrow C_nH_{(2n+2)} + nH_2O \quad (1)$$

The FT process can be potentially used in synthesis of chemicals with high commercial value, such as light olefins [1,2], alcohols [3,4] and other oxygenates [5]. The yield of products with secondary functional group (i.e., OH or unsaturated bond) is usually low. The FT process is preferentially conducted at moderate conditions, 473–573 K and 10–60 bar, to reach high product selectivity [6].

Due to the abundance of conventional and unconventional gas reserves rich in $CH_4$ (i.e., tight and shale gas, methane hydrate, coalbed methane), which have recently been discovered, $CH_4$ constitutes the most promising fossil feedstock for fuels and chemicals production through FT.

Therefore, many $CH_4$ reforming routes resulting in different product distributions have been investigated: non-oxidative methane coupling, pyrolysis, partial oxidation, steam and dry reforming are of great interest [7].

Dry methane reforming (DMR) has attracted interest because it can valorize the abundant and cheap natural gas and reduce the carbon footprint due to the increasing fossil fuel consumption worldwide [8]. In DMR, $CO_2$ is used as oxidizing agent, and so $CH_4$ is oxidized to CO whilst $H_2$ is formed at relatively high temperature.

Significant effort has been put on catalyst synthesis to improve the reaction efficiency. Numerous catalysts have been developed aiming at maximizing syngas yield at lower temperatures. Mostly Nickel and noble metals (i.e., Pt, Ru, and Rh) have been investigated as potential catalysts for DMR. Noble metals show high activity and resistance against carbon formation [9–12]. Although they reach excellent performance, high cost is the main constraint towards their industrial application. Alternatively, nickel-based catalysts may be used. However, they face deactivation issues due to sintering and carbon encapsulation of Ni under reforming conditions [13].

Application of non-equilibrium gas phase electrical discharges, where energy is channeled into molecular dissociation instead of gas heating, is an encouraging alternative. Besides the low operating temperatures, plasma application for $CO_2$ and $CH_4$ dissociation is also considered as a way for green electricity storage into chemical bonds. DMR has been explicitly studied in dielectric barrier discharges (DBD) [14–17]. Mainly syngas and light hydrocarbons and oxygenates are formed; however, neither conversion rate, nor the global energy efficiency is high. On the contrary, repetitive pulsed excitation with a nanosecond scale pulse rise time and duration appears to be a better alternative due to its highly non-equilibrium nature [18].

DMR is an appealing route to valorize natural gas and reduce $CO_2$ emissions and this is reflected in numerous works either on thermal catalytic or plasma-assisted DMR. Both processes have strengths and downsides. This work strives to compare, for first time in the literature, the plasma-assisted DMR process with the thermal catalytic DMR for production of syngas with composition suitable for methanol synthesis through an FT process ($H_2/CO \geq 2$ in mole). Both processes are conceptually designed and simulated in the Aspen Plus process simulator. Different process steps are investigated. Heat integration and equipment cost estimation are performed for the most promising process flow diagrams. Eventually, a comparison between the two processes is conducted based on quantitative (resource efficiency, utility demand and capital cost) and qualitative (complexity, compatibility and sustainability) performance criteria.

## 2. Materials and Methods

Utilities, operating and maintenance as well as capital investment are the major costs of syngas production (after the raw material cost) corresponding to ~7%, 16% and 10%, respectively, of the total production cost [19]. The syngas production cost has a great impact on the economic feasibility of gas-to-liquid (GTL) fuels and chemicals [20] and is vital for the commercialization of GTL processes. Capital investment and operating costs (i.e., utility, maintenance, general expenses and plant overhead costs) strongly depend on the process design and the engineering. Therefore, process block diagrams (PBD) for syngas production achieving molar ratio of $H_2/CO \geq 2$ at industrial scale are developed for both thermal catalytic and plasma-assisted DMR processes. Different process steps are designated and simulated in the Aspen Plus process simulator V8.8 for each PBD. The utility demand is reported while the cost of each piece of equipment is estimated. The utility demand is distinguished in cold and hot utility and expressed in $kWh/kmol_{syngas}$. The type and cost of process equipment that is required for syngas production is correlated with the maintenance/operation and capital expenditure. Eventually, the PBDs are evaluated with respect to the utility demand and required process equipment (type of equipment and cost) to define the most promising process flow diagram (PFD), which leads to the lowest syngas production cost.

### *2.1. Process Modeling*

All process units are simulated according to experimental data published in the literature assuming chemical and thermodynamic equilibrium. The sizing of the process equipment is facilitated by mass and energy balances, design equations and rules of thumb. The process model development, and the calculation of the mass and energy balances for both processes are based on the following design inputs:

- The boundary limits are set on the dry methane reforming process itself. Intermediate steps of the input streams ($CH_4$ and $CO_2$) such as transportation, purification and $CO_2$ capture are beyond the scope of this work since they are common steps for both processes. Thus, they can be excluded in a relative comparison. Therefore, reactants are considered to be free of impurities. Although extremely high purity streams are difficult to be achieved in reality, plasma-assisted processes are tolerant to impurities presence. Since plasma chemistry occurs in the gas phase reaction and no catalyst is involved, impurities do not affect the plasma reactor performance. In addition, impurities concentration may be reduced during the plasma reaction since they are cracked by the electrons [21].
- The predictive Redlich–Kwong–Soave (PSRK) equation of state is selected to calculate all the thermodynamic properties for the components involved in the overall process. This thermodynamic model provides high accuracy in water-hydrocarbon systems over a wide range of temperatures and predicts the instability of the liquid phase [22].
- An equimolar total feed is set for the simulation. The chosen feed rate produces a certain amount of syngas, which can be utilized for small-size methanol production (plant design capacity of 100–200 $kt_{MeOH}/y$) since dry methane reforming processes (both plasma-assisted and thermal catalytic) have not been established at large industrial scale yet [8,23]. Therefore, the lowest industrial capacity is selected. Equimolar feed is selected because this is the feed composition adopted in most of experimental works as well as in the work that will be used as reference case in the plasma-assisted process. Moreover, the data obtained from the literature to facilitate the comparison among the different process alternatives are coherent since they correspond to the same plant capacity (500–1000 kmol/h). It is assumed that 500 kmol/h of $CH_4$ are available for the plasma-assisted process and 1000 kmol/h for the thermal catalytic one because steam methane reforming (SMR) is also required in the later process to achieve the targeted syngas composition; regarding the thermal catalytic process, 312.5 kmol/h are consumed in DMR and the rest in SMR.
- The reactor model which minimizes the Gibbs free energy (known as RGIBBS reactor model in Aspen Plus process simulator) is used to simulate the thermal catalytic reactors of DMR, water-gas shift (WGS), SMR and combined steam/carbon dioxide methane reforming (SCMR) at steady state. The reactor model where stoichiometry and molar extent can be defined when they are known for each reaction (known as RSTOIC reactor model in Aspen Plus process simulator) is used to simulate the plasma reactor at steady state.
- The thermal catalytic DMR reactor achieves chemical equilibrium at 750 °C and pressure equal to 1 bar in order to simulate the results achieved by Theofanidis et al. [24]. These authors synthesized a bimetallic Fe-Ni/$MgAl_2O_4$ catalyst with enhanced carbon-resistance (about 4 h stable performance) and relatively low catalyst demand ($W_{cat}/F_{CH4}$ = 800–1420 kg s $mol^{-1}$) suitable for DMR at the aforementioned conditions; approximately 1.3% of $CH_4$ feed results in coke formation. For high energy efficiency, the WGS reaction occurs at the same conditions as thermal catalytic DMR. Therefore, the WGS reactor also achieves chemical equilibrium at 750 °C and pressure of 1 bar; Fe-based catalysts promote the reaction and low catalyst load in the reactor is required ($W_{cat}/F_{tot}$ = 0.04 kg s $mol^{-1}$) [25,26]. The thermal catalytic SMR reactor is at chemical equilibrium at 1000 °C and pressure of 1 bar. Ni- and Ru-based catalysts enhance the reaction at catalyst demand of $W_{cat}/F_{CH4}$ = 250 kg s $mol^{-1}$ [27,28]. The thermal catalytic SCMR reactor is also at chemical equilibrium at 1000 °C and pressure of 1 bar [29]. A low amount of Ni-MgO-$Ce_{0.8}Zr_{0.2}O_2$ catalyst is used ($W_{cat}/F_{CH4}$ = 20 kg s $mol^{-1}$) to enhance the reaction [30].
- The results obtained by the plasma-assisted process models are based on linear extrapolation of the experimental data, regarding flow rates, conversions and energy input, reported by

Scapinello et al. [31]. In particular, the authors [31] used a nanosecond repetitive pulsed discharge to dissociate $CH_4$ and $CO_2$ achieving 40% energy efficiency for syngas production, a value that is among the highest ones achieved with other discharges in the literature. Conversions of approximately 50% and 42.5% for $CH_4$ and $CO_2$, respectively, are reported. The specific energy input is approximately 10 kJ/$L_{FEED}$ while the 14% of the carbon in the feed is transformed to coke.

- The hot and cold utility demand and the electricity consumption are expressed in kWh/$kmol_{syngas}$, while the equipment cost is expressed in k$/($kmol_{syngas}$ $h^{-1}$) in order to facilitate the technology comparison. Since hot/cold utilities and electricity price vary, no specific values are used; rather, hot/cold utilities and electricity are expressed in kWh/kmol of syngas. The specific syngas production cost (k$/kmol) may be calculated by multiplication of this ratio with the cost of kWh.
- The composition of the final syngas stream prior to Fischer-Tropsch unit is required to be at a temperature of 250 °C, pressure of 30 bar and composition of $H_2/(2CO + 3CO_2) \geq 1$ to promote methanol production reactions:

$$CO + 2H_2 \rightarrow CH_3OH \qquad \Delta H° = -90.77 \text{ kJ/mol}, \tag{2}$$

$$CO_2 + 3H_2 \rightarrow CH_3OH + H_2O \quad \Delta H° = -49.16 \text{ kJ/mol} \tag{3}$$

- Methanol is an important chemical compound. It can be used as fuel and feedstock to synthesize olefins or it can be blended with gasoline and diesel. The production of methanol is especially attractive in emerging economies as a liquid fuel to replace conventional sources of energy.
- The temperature of the compressors in the inlet streams does not exceed 50 °C in order to avoid very high temperatures at the outlet after compression. High temperatures may result in equipment damages. The outlet streams of the thermal reactor are not cooled down in order to create a very hot stream after the compression that can be used for heat integration purposes. Moreover, cooling of those streams result in water condensation prior to compression.
- A heat transfer coefficient 0.5 kw/$m^2$ °C for gas-to-gas heat exchange is used for the heat exchange area estimations. A polytropic compression ASME efficiency of 75% is assumed.

The process flow diagram (PFD) and the detailed mass and energy balances of plasma-assisted and thermal catalytic DMR processes are presented in the Supplementary Materials.

### *2.2. Thermal Catalytic DMR Process*

Purified streams of $CH_4$ and $CO_2$ are fed to the thermal catalytic reactor where the DMR reaction occurs:

$$CH_4 + CO_2 \leftrightarrow 2CO + 2H_2 \qquad \Delta H° = 261 \text{ kJ/mol} \tag{4}$$

The RGIBBS reactor model (minimization of Gibbs free energy) is used to simulate the thermal catalytic reactor at steady state. Chemical equilibrium is achieved at 750 °C and 1 bar. $CH_4$ and $CO_2$ conversion of 85% and 90%, respectively, are achieved at these conditions. $CO_2$ conversion is higher than $CH_4$ conversion because the reversed water-gas shift (RWGS) reaction occurs concurrently in the reactor:

$$CO_2 + H_2 \leftrightarrow CO + H_2O \quad \Delta H° = 41 \text{ kJ/mol} \tag{5}$$

Thus, slightly higher amount of CO is produced compared to the stoichiometry of the reaction. The amount of $H_2$ produced is also slightly higher than that dictated by the stoichiometry due to coke formation that occurs simultaneously with DMR. The coke is mainly formed through the following reactions [32]:

$$CH_4 \rightarrow C + 2H_2 \qquad \Delta H° = 75 \text{ kJ/mol} \tag{6}$$

$$2CO \rightarrow C + CO_2 \qquad \Delta H° = -172 \text{ kJ/mol} \tag{7}$$

The composition of the DMR reactor outlet stream after considering all the aforementioned side reactions occurring in the reactor are presented in Table 1. The $H_2$/CO molar ratio in the DMR outlet

stream is 0.94. A gas separator (pressure swing adsorption, absorption and membrane) could be used to separate the two gases, $H_2$ and CO, and afterwards, the two gas streams could be mixed again in volumetric ratio of $F_{H2}/F_{CO} = 2$ in order to achieve the targeted molar ratio for the methanol synthesis reaction. Pressure swing adsorption (PSA) gives high separation efficiency and is widely used in industry but low $H_2$ recovery [33], especially at streams with low $H_2$ content, and high gas loss from the pressure release during desorption could be considerable disadvantages [34]. Absorption of CO is a well-known process resulting in high purity and recovery of CO, but the nature of the solvent (cuprous chloride, hydrochloric acid and water) is associated with technical challenges (corrosion, safety issues, high reactivity, etc.). Next to that, high pressure and low temperature, which enhance both the absorption process and solvent recovery, have a significant impact on the operating and capital costs. Membranes are suitable for $H_2$ purification but practical issues, such as membrane stability, mass transfer limitations and high costs related to operation, capital investment and maintenance are considerable limitations for a large-scale, cost-efficient separation [35]. In addition, half of the produced CO would remain unutilized in methanol synthesis thus resulting in lower resource efficiency. However, the $H_2$/CO molar ratio can be adjusted to the targeted ratio by co-feeding water (steam) in the DMR reactor. This reaction is known as combined steam and carbon dioxide methane reforming (SCMR), or bi-methane reforming (BMR) [36,37]. Since SCMR is an extremely energy intensive reaction [38] and the focus of the current work is on the study of DMR as main source of syngas, this scenario is not investigated. However, water (steam) and the DMR outlet stream react in a WGS reactor, connected in series with the DMR reactor and operating at the same conditions (T = 750 °C; P = 1 bar) [29] to promote heat integration and boost the energy efficiency of the process. Moreover, operating at lower temperature (i.e., 400–600 °C), would lead to CO conversion increase and consequently to higher amounts of $H_2$ and $CO_2$ and a ratio of $H_2/(2CO + 3CO_2) \leq 1$ in the final syngas stream. In the latter case, a liquefaction temperature lower than −10 °C would be needed to remove the higher excess of $CO_2$ and yield the targeted ratio of $H_2/(2CO + 3CO_2) \geq 1$ in the final syngas stream. Such decrease in the liquefaction temperature would have major impact on the energy consumption of the process. The following reaction, known as water-gas shift (WGS) reaction, takes place in the WGS reactor:

$$CO + H_2O \leftrightarrow CO_2 + H_2 \quad \Delta H° = -41 \text{ kJ/mol} \tag{8}$$

**Table 1.** Dry methane reforming (DMR) and water-gas shift (WGS) reactor inlet and outlet streams composition.

| Stream | 1 | | 2 | | 3 | | 4 | |
|---|---|---|---|---|---|---|---|---|
| | Feed | | DMR Outlet | | Water (Steam) | | WGS Outlet | |
| Component | kg/h | kmol/h | kg/h | kmol/h | kg/h | kmol/h | kg/h | kmol/h |
| $CO_2$ | 13,753 | 312.5 | 1315 | 30 | - | - | 7739 | 176 |
| CO | - | - | 15,246 | 544 | - | - | 12,281 | 438 |
| $H_2O$ | - | - | 377 | 21 | 7251 | 403 | 4276 | 237 |
| $H_2$ | - | - | 1013 | 503 | - | - | 1576 | 782 |
| $CH_4$ | 5013 | 312.5 | 815 | 51 | - | - | 107 | 7 |
| Total | 18,766 | 625 | 18,766 | 1149 | 7251 | 403 | 25,979 | 1640 |
| Volume flow ($m^3$/h) | 15,451 | | 97,722 | | 34,236 | | 139,509 | |
| Pressure (bara) | 1.0 | | 1.0 | | 1.0 | | 1.0 | |
| Temperature (°C) | 25 | | 750 | | 750 | | 750 | |

The RGIBBS reactor model is also used to simulate the WGS reactor at steady state. Chemical equilibrium is also achieved at 750 °C and 1 bar. The amount of steam that is added to promote the WGS reaction has been defined after a sensitivity analysis, setting as objective the molar ratio of $H_2$/CO to be equal to 2 at the WGS outlet stream (Figure 1). Co-feeding of 14,502 kg/h of water (steam) results in the targeted ratio. However, it has been noticed that, only in the thermal catalytic process, even lower water amount (7251 kg/h) can be fed in WGS and still meet the targeted syngas composition at the end of the process. This is possible since the SMR controls the $H_2$/CO ratio, thus,

it is not necessary the $H_2/CO$ to be equal to 2 at the WGS outlet stream. Therefore, co-feeding of 7251 kg/h steam (2974 kg/h of fresh water and 4277 kg/h of water recycled from the compression section) are fed in the WGS.

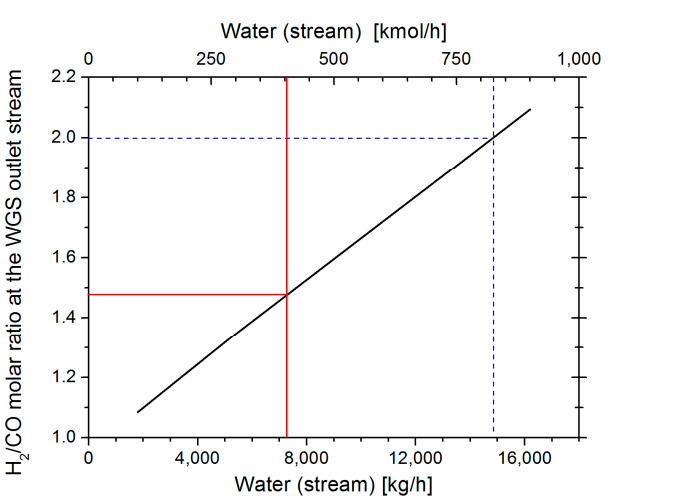


**Figure 1.** Sensitivity analysis of the amount of water (steam) on the $H_2/CO$ molar ratio in the water-gas shift (WGS) outlet stream; approximately 15 ton/h of water are required in the WGS reactor to reach $H_2/CO = 2$ at the outlet WGS stream.

CO and $H_2O$ conversion of 19.5% and 41.2%, respectively, are achieved at those conditions in the WGS reactor. The composition of the WGS reactor outlet stream is presented in Table 1. The combined DMR and WGS constitutes the upstream part (reaction section) that is common for all thermal catalytic process alternatives. The upstream part is presented in Figure 2.

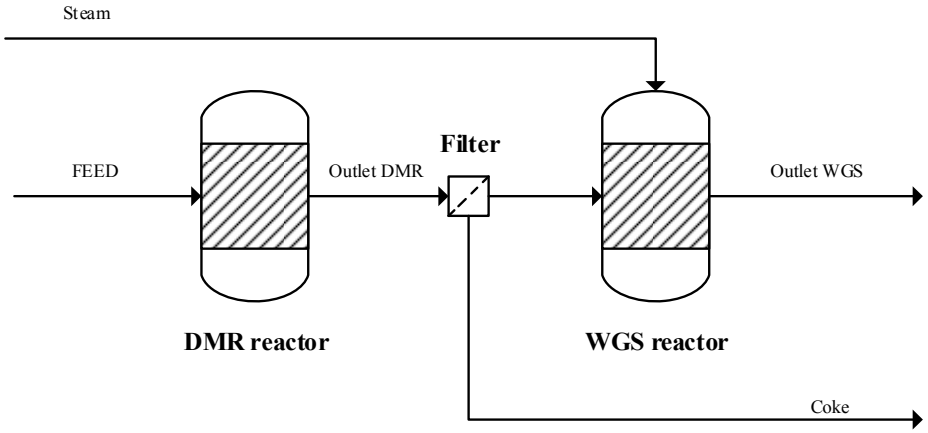


**Figure 2.** Upstream part (reaction section) of thermal catalytic dry methane reforming (DMR). $CO_2$ and $CH_4$ are cracked in the DMR reactor; $H_2O$ is added in a second step to the water-gas shift (WGS) reactor to adjust the $H_2/CO$ ratio in the final syngas stream.

Since considerable differences have been reported between the experimental and theoretical equilibrium constants ($K_{eq}$) of the WGS reaction [39–41], a sensitivity analysis has been performed to investigate the effect of $K_{eq}$ at 750 °C on $H_2/CO$ and $H_2/(2CO + 3CO_2)$ (Figure 3). Figure 3 shows that, when $K_{eq}$ varies from 0.45 to 1.3, the ratios $H_2/CO$ and $H_2/(2CO + 3CO_2)$ (process targets) remain practically unaffected.

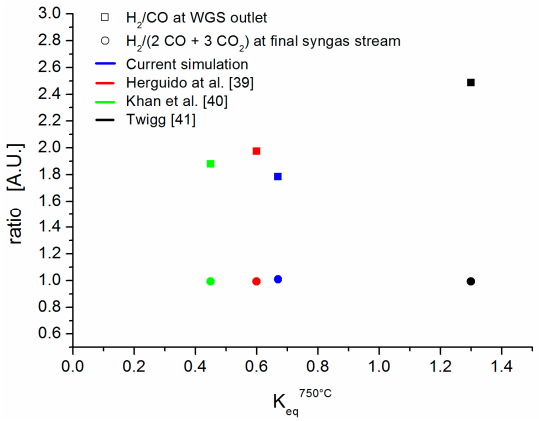


**Figure 3.** Sensitivity analysis of the equilibrium constant for the water-gas shift (WGS) reaction at 750 °C. The effect of the experimental equilibrium constants reported by Herguido et al. [39] and Khan et al. [40], the theoretical one reported by Twigg [41], and the theoretical one calculated by Aspen Plus process simulator V8.8 (this work) on the $H_2/CO$ and $H_2/(2CO + 3CO_2)$ ratio of the WGS outlet and final syngas stream, respectively, is shown.

The WGS reactor outlet stream flows towards the downstream part of the process in order to be purified prior to being fed into the FT process. A considerable amount of $CO_2$ is produced after the WGS reaction; thus, it needs to be separated from the entire gas mixture to achieve the targeted stream composition of $H_2/(2CO + 3CO_2) \geq 1$.

Absorption (both chemical and physical absorption), adsorption, membrane separation and cryogenic processes are well-studied carbon capture and storage (CCS) processes. Chemical and physical absorption (i.e., amine process and Selexol solvent, respectively) have drawn considerable attention due to their relatively high technical maturity and feasibility for large scale capacities. However, challenges, such as solvents chemical instability and high energy requirements for solvent regeneration [42] should be taken into account. The adsorption and membrane processes are also considered promising CCS technologies due to their potential for lower energy consumption for $CO_2$ separation compared to absorption. However, capacity limitations, high capital investment and lower separation efficiency compared to absorption (lower $CO_2$ purity and recovery) are important disadvantages [43–46]. The cryogenic separation process attains high separation efficiency and compression and refrigeration systems are well-established at large scale. Nevertheless, extremely low temperature and high compression rates increase substantially the operation cost [47] and many efforts are currently devoted to process optimization and energy requirement reduction [48,49].

Considering the strengths and weaknesses of the aforementioned CCS technologies as well as their technology readiness level and maturity at large scale capacities, $CO_2$ absorption using amines and cryogenic separation are selected as downstream process sections in a thermal catalytic DMR process for syngas production. Two PBDs are developed and evaluated below.

### 2.2.1. Thermal Catalytic DMR Process with $CO_2$ Absorption (Amine Process)

In this scenario, the excess of $CO_2$ is captured in an absorber using monoethanolamine (MEA) [50]. The WGS reactor outlet stream enters from the bottom of the absorber and comes in contact with an aqueous MEA solution, which enters from the top and flows counter-currently to the WGS reactor outlet stream. $CO_2$ reacts exothermically with MEA and form a water-soluble salt. The released heat is absorbed by the fresh streams that enter the column. The temperature and pressure of the column are ~57 °C and 3.4 bar, respectively. The rich in salt MEA stream exits the absorber from the bottom of the column, while the free of $CO_2$ stream exits from the top. The rich MEA stream is preheated in a heat exchanger by the regenerated MEA stream from the stripper (heat integration to reduce the energy cost) and enters the stripper where the salt formation reaction is reversed by supplying additional heat. The temperature and pressure of the stripper column are 110–120 °C and 2 bar, respectively. In the stripper, $CO_2$ is degassed from the MEA stream and gets off from the top of the

stripper column, whereas the regenerated MEA stream gets off from the bottom. Consequently, $CO_2$ and MEA are recycled back to the DMR reactor and the absorber, respectively. The PBD of the process and the process flow diagram of this downstream process alternative are presented in Figure 4.

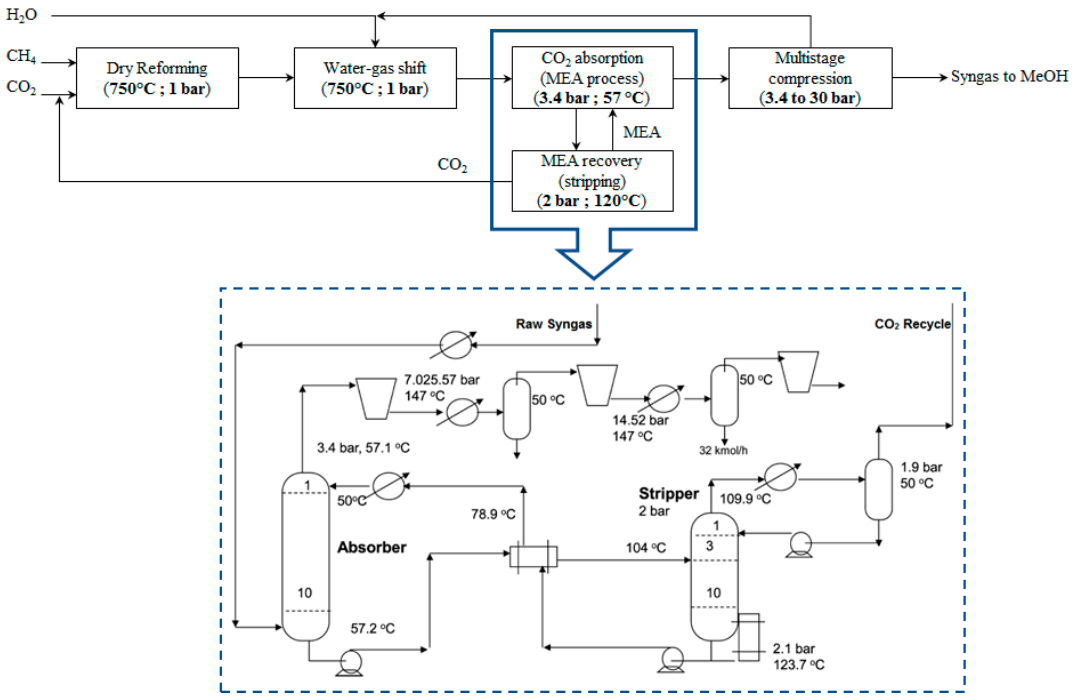


**Figure 4.** Process block diagram and process flow diagram of a thermal catalytic dry methane reforming (DMR) process using a monoethanolamine (MEA) process for $CO_2$ absorption [51].

Absorption of $CO_2$ using MEA has been extensively studied and simulated [52,53]. The economic potential of the process has also been evaluated and compared with other peer $CO_2$ capture technologies [54]. Recently, Luyben [51] designed a DMR process for syngas production. He developed and evaluated two process alternatives: one without $CO_2$ recycle, thus no separation section was included, and one with $CO_2$ recycle, therefore an absorber with aqueous MEA solution and a stripper for solvent regeneration was included. He concluded that the scenario of $CO_2$ recycle results in lower total annual cost than the scenario without $CO_2$ recycle and notably, the total annual cost is minimized when the reactor pressure is at 4 bar. Approximately 5.6 kWh/kmol$_{syngas}$ cold utility, 2.6 kWh/kmol$_{syngas}$ hot utility, 2.4 kWh/kmol$_{syngas}$ of electrical power and 6.6 k\$/(kmol$_{syngas}$ h$^{-1}$) are required for syngas purification when adopting this process alternative.

### 2.2.2. Thermal Catalytic DMR Process with $CO_2$ Liquefaction (Cryogenic Separation)

In this scenario, a cryogenic process is employed for $CO_2$ excess removal. The WGS reactor outlet stream is initially compressed to 30 bar, a suitable pressure for the Fischer-Tropsch process. Moreover, pressure increase facilitates the cryogenic separation as the liquefaction temperature increases too. Almost all $H_2O$ is condensed and removed after the first compression stage; the compressed stream at 5 bar is cooled down to 20 °C and flashed in a knock-out drum (vapor–liquid separators). The stream is further compressed to 15 bar and cooled down firstly by the liquid stream coming from the knock-out drum and consequently, by an external cold utility. Part of the $CO_2$ is liquefied and recovered from the drum. The stream is further pressurized to 30 bar, cooled down to −115 °C and flashed. Under such conditions, almost the entire amount of $CO_2$ is liquefied and removed from the stream. The cold purified syngas stream can be integrated in the process and be used as cold utility. The PBD of the process and the process flow diagram of this downstream process alternative are presented in Figure 5.

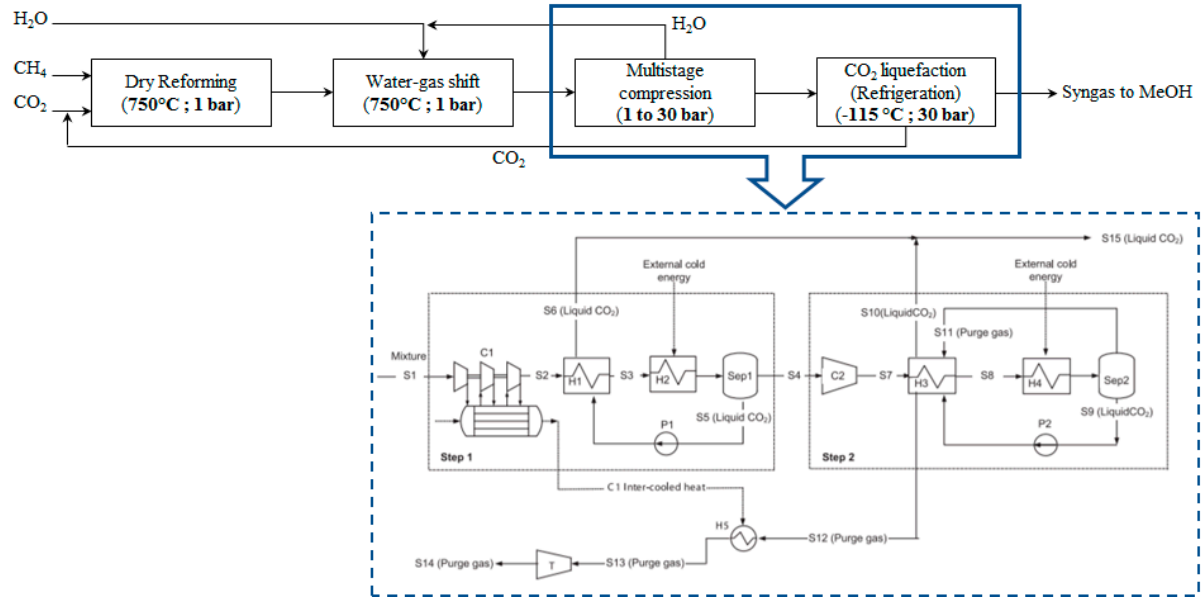


**Figure 5.** Process block diagram and process flow diagram of a thermal catalytic dry methane reforming (DMR) process with cryogenic separation process [55] ($CO_2$ liquefaction process).

Cryogenic separation is not only used in oil and gas industry for light hydrocarbons separation [56,57], but also for synthetic natural gas purification [47,58]. Although cryogenic separation requires no chemical agents, the extreme operating conditions require high energy consumption, which is a major drawback. Especially when gases with lower boiling points ($H_2$, $CH_4$, and CO) are present, the phase transition temperature of $CO_2$ drops to values even lower than −80 °C and the refrigeration energy becomes the main cost driver of the separation. The effect of $CO_2$ concentration on the phase transition temperature is presented in Figure 6.

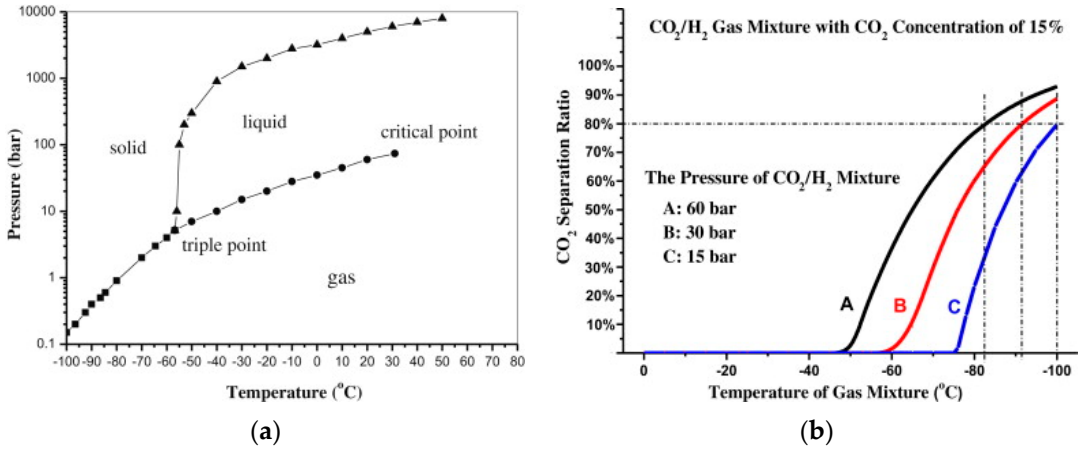


**Figure 6**. $CO_2$ phase transition temperature: (**a**) Pure $CO_2$ stream; and (**b**) $CO_2/H_2$ gas mixture with 15% (molar base) $CO_2$ concentration [55].

Simulating this scenario in the Aspen Plus process simulator V8.8, it is found that the $CO_2$ phase transition temperature in the syngas stream (14.4% $CO_2$, 28.7% CO and 56.9% $H_2$) at a pressure of 30 bar is −115 °C for 99.2% recovery, result which is in accordance with Figure 6b. Based on the simulation results, ~5.3 $kWh/kmol_{syngas}$ cold utility, 3.1 $kWh/kmol_{syngas}$ hot utility and 7.9 $kWh/kmol_{syngas}$ electrical power are required for syngas purification. The capital investment of the $CO_2$ liquefaction process is lower than the MEA absorption process and similar to Selexol™ absorption process [55]. Xu et al. [47] have also compared the total capital investments of a $CO_2$ liquefaction process over the Selexol™ process and concluded that the first is about 40% less expensive than the second one. Thus, the capital investment of the $CO_2$ liquefaction process is about

4 k$/(kmol$_{syngas}$ h$^{-1}$) including the compression section and the refrigeration system needed to achieve the required operating temperatures.

### 2.2.3. Thermal Catalytic DMR Process Integrated with SMR

Removal of $CO_2$ from the WGS outlet reactor stream increases the syngas production cost. Avoidance of implementation of $CO_2$ separation processes might increase the economic potential of syngas production. Additional gas conditioning units can be used instead of the energy and capital-intensive CCS technologies. In this scenario, steam methane reforming (SMR) is implemented in the process as an additional conditioning unit to tune the final syngas composition. Water (steam) reacts with $CH_4$ according to the following reaction:

$$CH_4 + H_2O \leftrightarrow CO + 3H_2 \qquad \Delta H° = 206 \text{ kJ/mol} \tag{9}$$

Syngas with different ratio than the WGS reactor outlet stream is produced in the SMR reactor. The two syngas streams are mixed and the final syngas composition attains the targeted molar ratio.

The RGIBBS reactor model is also used to simulate the SMR reactor at steady state. Chemical equilibrium is achieved at 1000 °C and 1 bar. Equimolar feed stream is assumed at the inlet of SMR reactor. The amount of methane and steam that is added to promote the SMR reaction has been defined after a sensitivity analysis, setting as objective the targeted molar ratio $H_2/(2CO + 3CO_2) \geq 1$ at the final syngas stream. A feed of 22,351 kg/h of methane and steam (10,528 kg/h of $CH_4$ and 11,823 kg/h of steam) results in achieving the targeted ratio. Conversion of 98.5% and 98.8% of $CH_4$ and $H_2O$ (steam), respectively, are achieved at these conditions in the SMR reactor. The PBD and the process flow diagram of this downstream process alternative are presented in Figure 7.

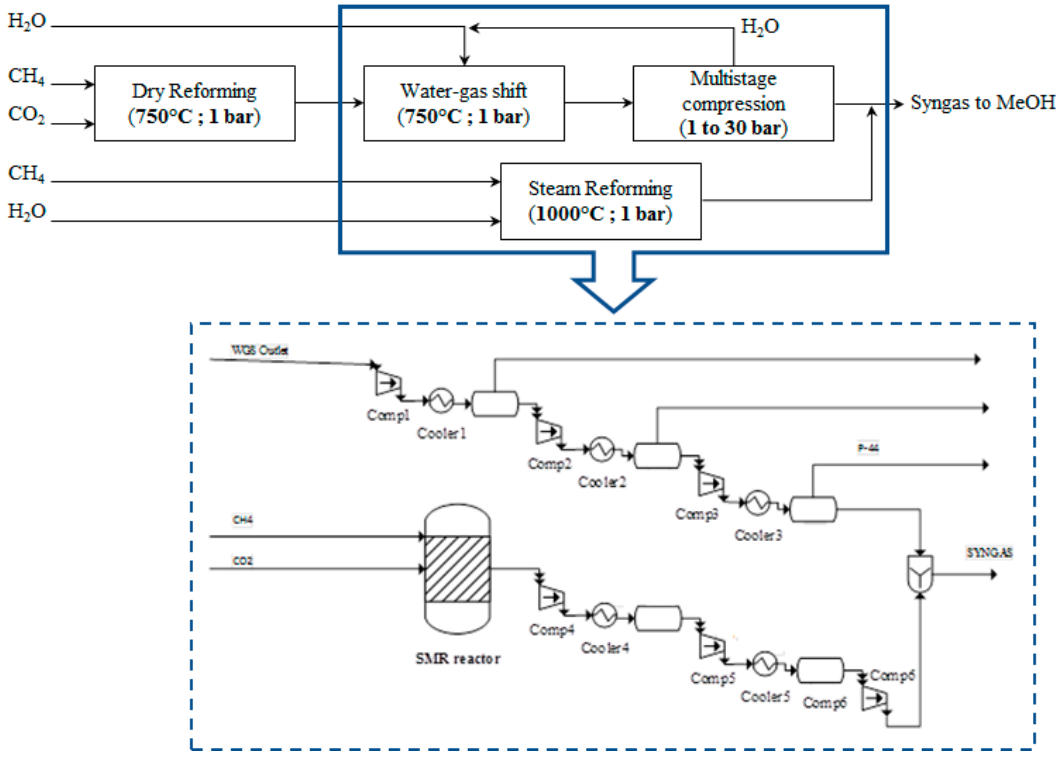


**Figure 7.** Process block diagram and process flow diagram of a thermal catalytic dry methane reforming (DMR) process with an SMR reactor and the respective process flow diagram.

Combination of DMR, WGS and SMR also in one step, known as combined steam-$CO_2$ methane reforming (SCMR), has been studied elsewhere [59,60] as a possible route for syngas production. Gangadharan et al. [61] concluded that a process combining dry methane reforming with steam methane reforming has comparable economic potential with the well-established SMR for syngas

production and lower carbon footprint. Basini and Piovesan [62] showed that this hybrid process is the most economical route to produce syngas with molar ratio of $H_2$/CO equal to 2. Based on the simulation results in the Aspen Plus process simulator V8.8, ~22.8 kW/($kmol_{syngas}$ $h^{-1}$) cold utility, 16.5 kW/($kmol_{syngas}$ $h^{-1}$) hot utility and 15.8 kWh/$kmol_{syngas}$ electrical power are required for syngas purification. It is worth mentioning that there is high potential of heat integration in this process, which will radically reduce the operating cost [63]. The capital investment of this process alternative is ~5.5 k$/($kmol_{syngas}$ $h^{-1}$); it includes the cost of compression section, which has been estimated at 5.4 k$/($kmol_{syngas}$ $h^{-1}$) by Luyben [51], and the SMR reactor cost, which has been estimated at 0.06 k$/($kmol_{syngas}$ $h^{-1}$) by Gangadharan et al. [61].

#### 2.2.4. Process Alternatives Evaluation for Thermal Catalytic DMR Process

In this section, the syngas purification process alternatives are evaluated based on their performance and the most competitive one is selected for the detailed design. The performance of each alternative is presented in Table 2.

**Table 2**. Performance criteria of the downstream process alternatives for thermal catalytic dry methane reforming (DMR) process.

| Purification Processes | Cold Duty kW/$kmol_{syngas}$ $h^{-1}$ | Hot Duty kW/$kmol_{syngas}$ $h^{-1}$ | Electricity kWh/$kmol_{syngas}$ | Capital Investment k$/(kmol $h^{-1}$) | Resource Efficiency $kmol_{syngas}/kmol_{CH4}$ |
|---|---|---|---|---|---|
| MEA absorption | 5.6 | 2.6 | 2.4 | 6.6 | 4.00 |
| $CO_2$ liquefaction | 5.3 | 3.1 | 7.9 | 4.0 | 3.91 |
| Combined DMR + SMR | 22.8 | 16.5 | 15.8 | 5.5 | 4.14 |

The MEA absorption process alternative requires the lowest amount of hot utility and electricity while the cold utility demand is almost the same as the $CO_2$ liquefaction process. The utilization of $CH_4$ to syngas is high too. However, it is the most capital-intensive process among the others, mainly due to distillation and stripping columns needed. Moreover, use of aqueous MEA solvents increases the environmental impact of the process. The $CO_2$ liquefaction process requires low cold and hot utility. Even though the cold duty is similar to the MEA absorption process, the actual cost is significantly higher because the operating temperatures are well below zero, so refrigerants as cooling media are required; in the other cases, cooling water is used since the operating temperatures are close to ambient. Considerable amount of electricity is required due to refrigeration system operation. No complex equipment is needed; therefore, the capital investment is low. Syngas losses due to purge streams, however, result in the lowest resource efficiency among the other process alternatives. The combined DMR + SMR process requires the highest cold and hot utility. In addition, ambient temperatures are targeted so cooling water can be used. High electrical power is required due to high flow rates of the process (steam is also added to promote the SMR reaction). The capital investment is relatively low since conventional equipment is used. The combined DMR + SMR process achieves the highest resource efficiency since syngas is the only product that is formed in the reformers and few separation steps are involved in the process, thus minimizing the material losses. Generally, the process design focus is on high resource efficiency (since raw material is the cost driver) and low capital investment. Low utility cost is also preferable but it is not a significant cost in syngas production cost as compared with the first two [19,64]. Based on the process evaluation, the combined SMR + DMR process is the most promising alternative. The economic potential of this process has been studied elsewhere [61,64].

### *2.3. Plasma-Assisted DMR Process*

Purified streams of $CH_4$ and $CO_2$ are fed in the plasma reactor powered by a repetitive nanosecond pulsed power generator, where plasma-assisted dry methane reforming (P-DMR) occurs. The most important electron impact reactions, which take place inside the plasma reactor are described elsewhere [65].

To develop the process flow diagram and evaluate the P-DMR process, the results obtained by Scapinello et al. [31] are linearly extrapolated at industrial capacities. This is a valid assumption considering that the industrial scale plasma reactors are bundles of small scale plasma reactor units [66], as it can be seen in Figure 8.

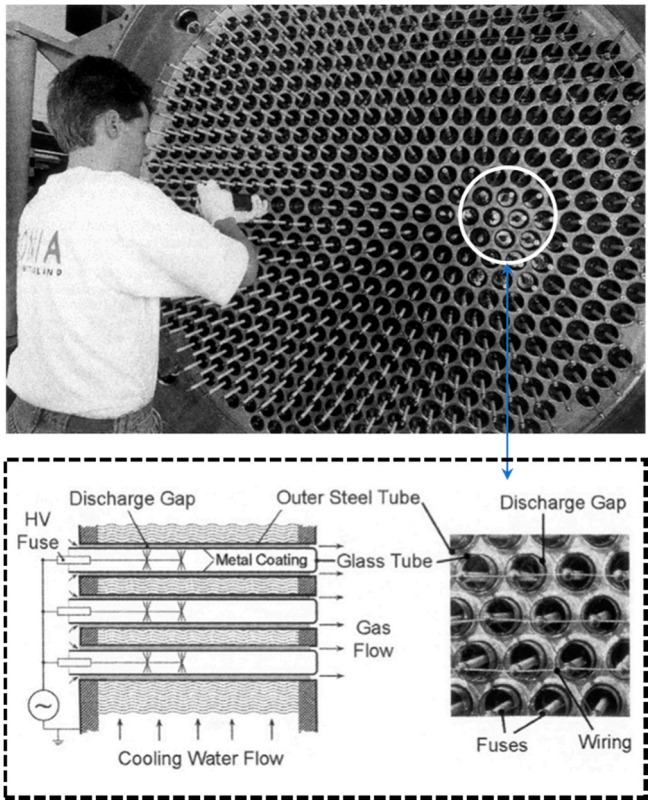


**Figure 8.** Plasma reactor at industrial scale as it is presented by Kogelschatz [66].

Therefore, the RSTOIC reactor model (stoichiometry and molar extent is known for each reaction) is used to simulate the plasma reactor at steady state. The temperature and pressure in the plasma reactor is 200 °C and 1 bar. $CH_4$ and $CO_2$ conversion of approximately 51% and 42.5%, respectively are achieved at specific energy input of 10 kJ/$L_{feed}$. $CH_4$ conversion of is higher than that of $CO_2$ because the dissociation energy of C-H bond (337.2 kJ/mol) is lower than the one of C=O (749 kJ/mol). Consequently, both high- and low-energy electrons may result in $CH_4$ dissociation, while only high energy electrons may result in $CO_2$ dissociation. Considering that the number of high energy electrons is lower than the number of low energy electrons in non-equilibrium plasma, the rate of $CH_4$ dissociation reactions is higher than that of $CO_2$. Thus, higher $CH_4$ conversion is observed in the P-DMR process.

The composition of the P-DMR reactor outlet stream after considering all the important plasma activated reactions are presented in Table 3. The $H_2$/CO molar ratio in the P-DMR outlet stream is 1.1. However, the molar ratio should be increased in order to reach the targeted value while unconverted reactants still need to be recovered from the stream and recycled back to the reactor.

**Table 3.** Plasma-assisted dry methane reforming (P-DMR) reactor inlet and outlet streams composition.

| Stream | 1 | | 2 | | 3 | | 4 | |
|---|---|---|---|---|---|---|---|---|
| | Feed | | P-DMR Outlet | | Water (Steam) | | SCMR Outlet | |
| Component | kg/h | kmol/h | kg/h | kmol/h | kg/h | kmol/h | kg/h | kmol/h |
| $CO_2$ | 22,005 | 500 | 12,595 | 286 | - | - | 14,171 | 322 |
| CO | - | - | 8095 | 289 | - | - | 16,445 | 587 |
| $H_2O$ | - | - | 2450 | 136 | 24,321 | 1350 | 20,110 | 1116 |
| $H_2$ | - | - | 647 | 321 | - | - | 2503 | 1242 |
| $CH_4$ | 8021 | 500 | 3979 | 248 | - | - | $2 \times 10^{-1}$ | $1 \times 10^{-2}$ |
| $C_2H_6$ | - | - | 75 | 2.5 | - | - | - | - |
| $C_2H_4$ | - | - | 175 | 6.25 | - | - | - | - |
| $C_2H_2$ | - | - | 879 | 33.8 | - | - | - | - |
| $C_3H_8$ | - | - | 14 | $3 \times 10^{-1}$ | - | - | - | - |
| Coke | - | - | 1117 | - | - | - | - | - |
| Total | 30,026 | 1000 | 30,026 | 1323 | 24,321 | 1350 | 53,229 | 3267 |
| Vol. Flow ($m^3$/h) | 24,721 | | 52,027 | | 105,861 | | 345,771 | |
| Pressure (bara) | 1.0 | | 1.0 | | 1.0 | | 1.0 | |
| Temperature (°C) | 25 | | 200 | | 1000 | | 1000 | |

The above-mentioned CCS technologies can be used for the unreacted $CO_2$ removal. Chemical absorption, membranes and adsorption technologies are mature and applicable to $CH_4$ removal. Even hybrid solutions (membrane and absorption based technologies) have been proposed and explicitly designed for this purpose [67]. Once the P-DMR outlet stream is purified and the targeted molar ratio is achieved ($H_2/CO \geq 2$), syngas may be fed in the FT process for methanol production.

Reactants removal can also be realized by secondary reactions; in this study, $CH_4$ can be further converted in a SCMR reactor into syngas simply by adding steam. Except for $CH_4$, a small amount of $CO_2$ also reacts with $H_2$ (RWGS reaction). Simultaneously, CO is converted to $H_2$ (WGS reaction) resulting in $H_2/CO$ molar ratio increase. Eventually, the whole $CH_4$ amount is converted to syngas in one reactor pass, while less $CO_2$ needs to be removed from the syngas stream prior to FT.

Two PBDs, which correspond to the above-mentioned separation alternatives, are developed and evaluated below.

#### 2.3.1. Plasma-Assisted DMR Process with $CH_4$ and $CO_2$ Removal

This process configuration is initially simulated in the Aspen Plus process simulator V8.8. The P-DMR outlet stream is compressed in two steps. First, it is compressed from atmospheric pressure to 30 bar to facilitate $CO_2$ removal by liquefaction; the stream is simultaneously cooled down to −100 °C. The liquid $CO_2$ is recovered from the bottom of a knock-out drum. The separation of $CH_4$ from $H_2$ and CO is accomplished by an absorption/stripping process [68] at industrial scale. The cooled, free-of-$CO_2$ stream is further compressed to 33 bar to enhance the solubility of $CH_4$ in the liquid $C_3H_8$, which is chosen as suitable solvent; the solubility of $CH_4$ in liquid $C_3H_8$ is the highest among the organic solvents, such as $C_4H_{10}$, $C_5H_{12}$, $C_6H_{14}$ and $C_8H_{18}$ [68]. The free-of-$CO_2$ stream enters the absorption column from the bottom and flows counter-currently with the solvent stream, which enters form the top. $CH_4$ is selectively dissolved and the rich-in-$CH_4$ stream leaves from the bottom of the column. The purified syngas stream escapes from the top. The solvent is regenerated in a stripping column at 30 bar where 80.5% of $CH_4$ is recovered. The stripper outlet stream is depressurized down to 10 bar and stripped further in a second stripping column where all the amount of $CH_4$ is recovered. Inevitably, ~15% of $C_3H_8$ is contained in the $CH_4$ stream; the remaining 85% of $C_3H_8$ is recycled back to the absorber. A third stripper, operating at 25 bar, is employed to recover the remaining amount of solvent, since $C_3H_8$ losses drive the economic viability of this separation process. It has been estimated that the separation is not economically viable for solvent losses higher than 6% [68]. In this process simulation, 99% of the solvent is recovered. Eventually, $CH_4$ and $C_3H_8$, which are separated in the last stripping tower, are recycled back to the plasma reactor and absorber, respectively. The excess of $CO_2$ is further removed in a $CO_2$ liquefaction process and

the targeted molar ratio ($H_2/(2CO + 3CO_2) \geq 1$) is attained. The PBD and the respective process flow diagram are presented in Figure 9.

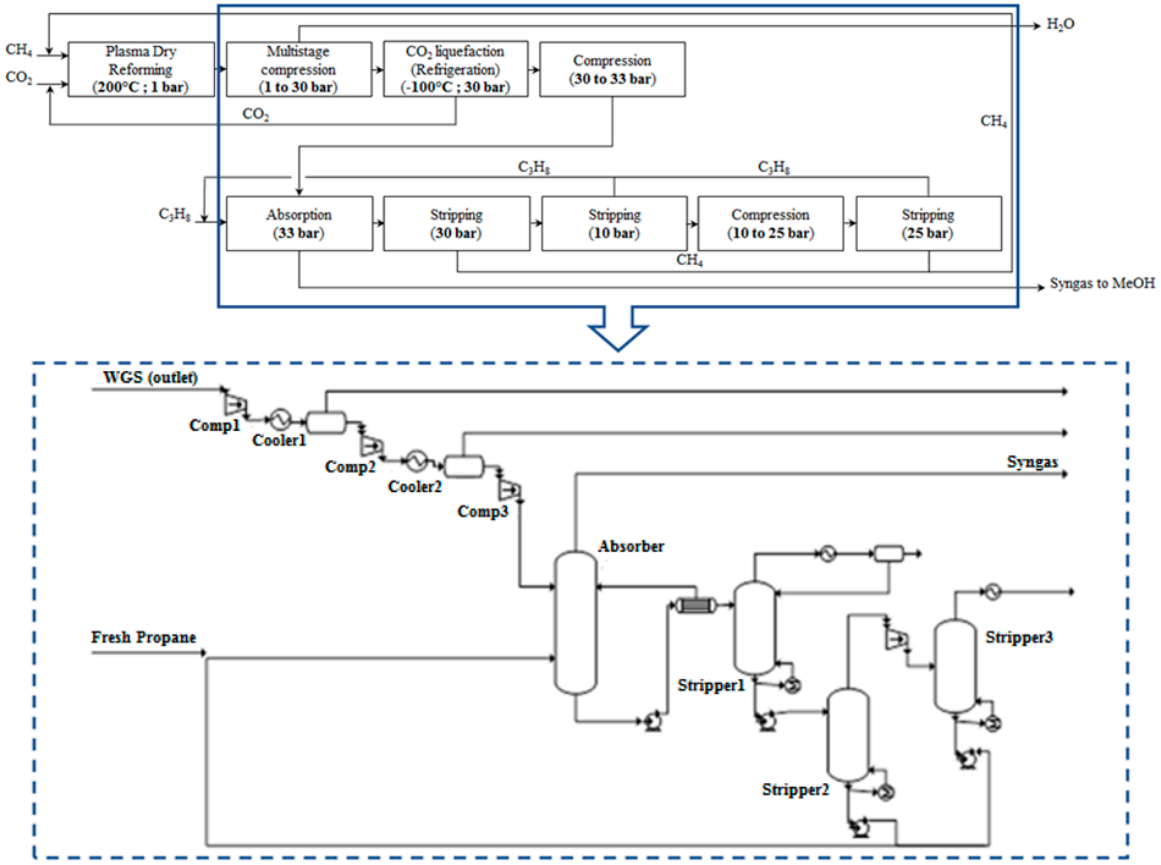


**Figure 9.** Process block diagram and process floe diagram of a plasma-assisted dry methane reforming (P-DMR) process with $CH_4$ and $CO_2$ removal processes.

### 2.3.2. Plasma-Assisted DMR Process Integrated with SCMR

Steam-$CO_2$ combined methane reforming (SCMR) is chosen in this scenario as a process alternative to "purify" the P-DMR outlet stream by adding water, thus, SCMR is promoted according to the following reaction:

$$3CH_4 + CO_2 + 2H_2O \leftrightarrow 4CO + 8H_2 \qquad \Delta H° = 659 \text{ kJ/mol} \qquad (10)$$

SCMR is a process with high industrial interest since syngas with $H_2/CO = 2$ molar ratio is produced that is suitable for gas-to-liquids [69] and catalysts have been synthesized to boost the reaction performance [59,60,70].

The RGIBBS reactor model is used to simulate the SCMR reactor at steady state. Chemical equilibrium is achieved at 1000 °C and 1 bar. The amount of steam that is added to promote the SCMR reaction has been defined after a sensitivity analysis, setting as objective the molar ratio of $H_2/CO$ to be at least equal to 2 at the SCMR outlet stream. According to Jang et al. [30], $(CO_2 + H_2O)/CH_4$ molar ratio higher than 1.2 (8.5 in this simulation), $CO_2/H_2O$ ratio higher than 0.47 (0.6 in this simulation) and a temperature higher than 850 °C (1000 °C in the simulation) are preferable reaction conditions for syngas preparation suitable for GTL processes. Co-feeding of 18015 kg/h of water (steam) results in the targeted ratio. $CH_4$, $CO_2$ and $H_2O$ conversion of 99.9%, 10% and 23.1%, respectively, are achieved at these conditions in the SCMR reactor. The composition of the SCMR reactor outlet stream is presented in Table 3. The excess of $CO_2$ is further removed in a $CO_2$ liquefaction process and the targeted molar ratio ($H_2/(2CO + 3CO_2) \geq 1$) is attained. The respective PBD as well as the process flow diagram are presented in Figure 10.

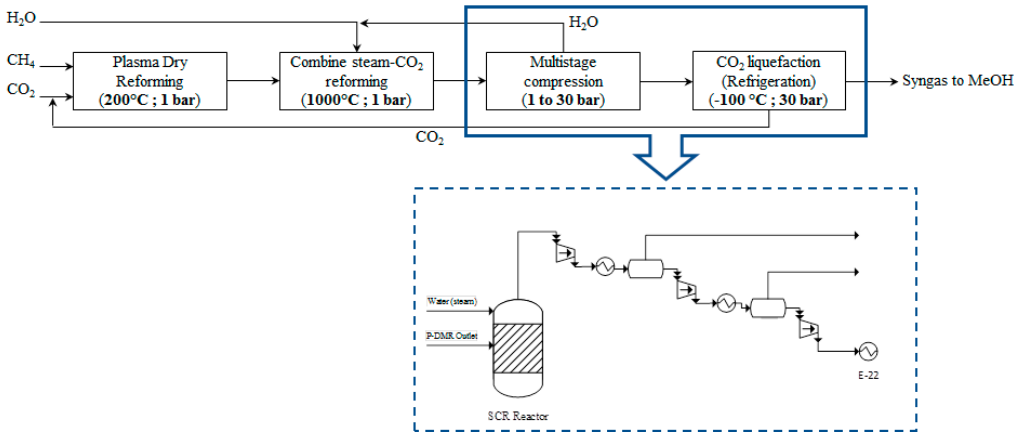


**Figure 10.** Process block diagram and process flow diagram of a plasma-assisted dry methane reforming (P-DMR) process with $CH_4$ and $CO_2$ removal processes.

2.3.3. Process Alternatives Evaluation for Plasma-Assisted DMR Process

The process alternative of $CH_4$ and $CO_2$ removal comprises eight process steps. Each process step requires unique process equipment while the feed throughputs are high; thus, the capital investment is foreseen to be high. Consequently, maintenance cost, which is assumed to be a fixed percentage of capital investment [71], is expected to be high, too, in this scenario. Moreover, temperature and pressure swing, which aim at solvent recovery together with high flow rate streams due to solvent use, increase the electricity demand, hot and cold duty in the process. This process certainly leads to highly complex process design.

The plasma-assisted DMR integrated with SCMR seems to be simpler process than P-DMR with $CH_4$ and $CO_2$ removal since it comprises four process steps. The capital investment and maintenance cost are foreseen to be lower due to less pieces of equipment, while constant pressure and temperature profiles mitigate the utility demand. In addition, higher $CH_4$ and $CO_2$ conversion is reached per reactor pas, which leads to higher resource efficiency. Collectively, plasma-assisted DMR integrated with SCMR is the most promising process alternative and is selected for the detailed design.

*2.4. Heat Integration*

Heat integration is performed in both thermal catalytic and plasma-assisted DMR process to recover and efficiently utilize all the available hot and cold process streams, thus, simulate a more relevant industrial environment. The hot and cold utility demand is minimized and a more realistic energy comparison between the two processes is conducted. Eventually, the respective heat exchanger network is designed with respect to the pinch analysis principles. The following assumptions are considered:

- The minimum temperature difference ($\Delta T_{min}$) is set at 20 °C
- The streams enthalpy is based on energy balances obtained by the process simulation.
- For the streams where phase change occurs during heating up, a pseudo $CP_M$ is calculated comprising the required energy both for evaporation and heating; the total stream enthalpy ($\Delta H$) is divided by the respective temperature difference.

In a thermal catalytic DMR process, five cold and six hot process streams are integrated to reduce the total hot and cold utility demand (Table 4). The total hot and cold utility demand before heat integration is 45.7 MW and 56.7 MW, respectively. The heat balances for the temperature intervals (Table 5) show that high surplus of energy is accumulated in the process. This fact is confirmed by the grand composite curve (GCC) (Figure 11) where the net heat flow against the shifted temperature is presented. A considerable energy pocket occurs in the process and proves the high potential of energy integration in thermal catalytic DMR process. The problem table algorithm for the required utilities (Table 6) reveals that ideally no hot utility is required to preheat the process streams at steady state. Heat is required only for the endothermic DMR, WGS and SMR reactions.

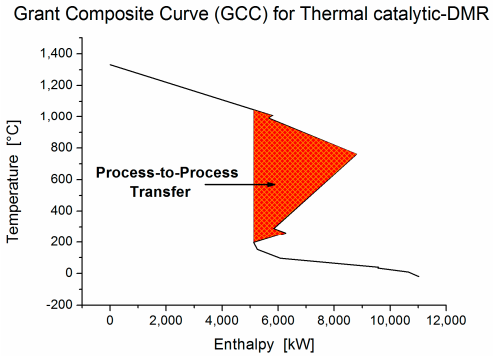


**Figure 11.** Grand composite curve of the thermal catalytic dry methane reforming (DMR) process. The energy pocket can be used for heating.

**Table 4.** Available process streams for heat integration in thermal catalytic dry methane reforming (DMR) process.

| Streams | | Actual Temperature °C | | Interval Temperature °C | | $CP_M$ kW/°C | ΔH kW | Total Demand MW |
|---|---|---|---|---|---|---|---|---|
| | | $T_{sup}$ | $T_{targ}$ | $T_{sup}$ | $T_{targ}$ | | | |
| FEED | Cold 1 | 25 | 750 | 35 | 760 | 9.0 | 6496 | 45.7 (Hot utility) |
| WATER to WGS | Cold 2 | 25 | 750 | 35 | 760 | 11.0 | 7945 | |
| $CH_4$ to SMR | Cold 3 | 25 | 1000 | 35 | 1010 | 11.2 | 10,901 | |
| $H_2O$ to SMR | Cold 4 | 25 | 1000 | 35 | 1010 | 15.3 | 14,920 | |
| Syngas | Cold 5 | 88 | 250 | 98 | 260 | 33.6 | 5441 | |
| Comp1 | Hot 1 | 1342 | 20 | 1332 | 10 | 18.1 | −23,883 | −56.7 (Cold Utility) |
| Comp2 | Hot 2 | 162 | 20 | 152 | 10 | 12.4 | −1767 | |
| Comp3 | Hot 3 | 104 | −10 | 94 | −20 | 12.6 | −1436 | |
| SMR-OUT | Hot 4 | 1000 | 50 | 990 | 40 | 22.1 | −20,967 | |
| CompSMR1 | Hot 5 | 299 | 50 | 289 | 40 | 21.3 | −5302 | |
| CompSMR2 | Hot 6 | 208 | 50 | 198 | 40 | 21.3 | −3368 | |

**Table 5.** Heat balances for the temperature intervals in thermal catalytic dry methane reforming (DMR) process.

| Temperature (°C) | Stream Overlapping | ΔT (°C) | $\Delta Cp_{(H,C)}$ (kW/°C) | ΔH (kW) | Surplus/ Deficit |
|---|---|---|---|---|---|
| 1332 | | 322 | −18.1 | −5817 | Surplus |
| 1010 | | 20 | 8.4 | 168 | Deficit |
| 990 | | 230 | −13.7 | −3140 | Surplus |
| 760 | | 471 | 6.3 | 2951 | Deficit |
| 289 | | 29 | −15.0 | −436 | Surplus |
| 260 | | 62 | 18.6 | 1151 | Deficit |
| 198 | | 46 | −2.8 | −127 | Surplus |
| 152 | | 54 | −15.2 | −821 | Surplus |
| 98 | | 4 | −48.8 | −195 | Surplus |
| 94 | | 54 | −61.4 | −3315 | Surplus |
| 40 | | 5 | 3.3 | 17 | Deficit |
| 35 | | 25 | −43.1 | −1078 | Surplus |
| 10 | | 30 | −12.6 | −378 | Surplus |
| −20 | | - | - | - | - |
| | C1 C2 C3 C4 C5 H1 H2 H3 H4 H5 H6 | | | | |

**Table 6.** Problem table algorithm for the required utilities in thermal catalytic dry methane reforming (DMR) process.

| T (°C) | Hot Utility | ΔH (kW) |
|---|---|---|
| 1332 | ↓ | 0 |
| | ΔH = −5817.2 kW | |
| 1010 | ↓ | 5817.2 |
| | ΔH = 168.3 kW | |
| 990 | ↓ | 5648.8 |
| | ΔH = −3140.2 kW | |
| 760 | ↓ | 8789.1 |
| | ΔH = 2951.0 kW | |
| 289 | ↓ | 5838.1 |
| | ΔH = −435.8 kW | |
| 260 | ↓ | 6273.9 |
| | ΔH = 1150.6 kW | |
| 198 | ↓ | 5123.3 |
| | ΔH = −126.9 kW | |
| 152 | ↓ | 5250.1 |
| | ΔH = −820.9 kW | |
| 98 | ↓ | 6071.0 |
| | ΔH = −195.2 kW | |
| 94 | ↓ | 6266.2 |
| | ΔH = −3314 W | |
| 40 | ↓ | 9580.9 |
| | ΔH = 16.5 kW | |
| 35 | ↓ | 9564.5 |
| | ΔH = −1077.6kW | |
| 10 | ↓ | 10,642.1 |
| | ΔH = −377.9 kW | |
| −20 | ↓ | 11,020.0 |
| | **Cold utility** | |

The heat exchanger network of the thermal catalytic DMR process is presented in Figure 12. Nine process-to-process streams heat exchangers and five coolers are required for the heat integration. Ideally, no hot utility demand is required. However, in the proposed heat exchanger network the $CH_4$ stream to SMR reactor needs to be heated from 847 °C to 1000 °C by an external heat source, even though there is still an amount of heat in the process, which could be used to satisfy this heat deficit. It has been estimated that two more heat exchangers should have been placed in the network to achieve that resulting in higher capital investment. Instead of designing a more expensive and complicated network, it is preferred to heat the stream up to 1000 °C in the SMR.

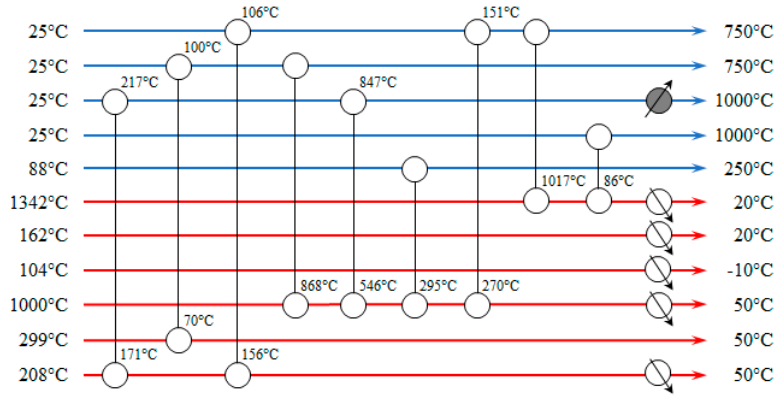


**Figure 12.** Heat exchanger network for the thermal catalytic dry methane reforming (DMR) process: in white, coolers for the hot process streams; and, in grey, the steam methane reforming (SMR) reactor.

In plasma-assisted DMR process, four cold and two hot process streams are integrated to reduce the total hot and cold utility demand (Table 7). The total hot and cold utility demand before heat integration is 48.8 MW and 72.8 MW, respectively. The heat balances for the temperature intervals (Table 8) show that there is a surplus of energy in the process that can be used for heating. This energy pocket gets noticeable in GCC (Figure 13) and is high enough to satisfy the heating requirements as it is shown in the problem table algorithm (Table 9). Eventually, no extra source of energy is required to preheat the streams at steady state; heat is required only for the endothermic SCMR reaction.

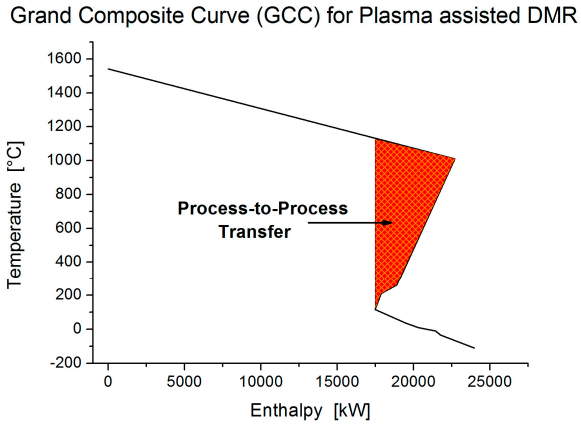


**Figure 13.** Grand composite curve of the plasma-assisted dry methane reforming (P-DMR) process. An energy pocket can be used to heat up the cold streams without needing an extra heat source.

**Table 7.** Available process streams for heat integration in the plasma-assisted dry methane reforming (P-DMR) process.

| Stream Name (Suppl. Material) | Stream Type | Actual Temperature °C | | Interval Temperature °C | | $CP_M$ kW/°C | ΔH kW | Total Demand MW |
|---|---|---|---|---|---|---|---|---|
| | | $T_{sup}$ | $T_{targ}$ | $T_{sup}$ | $T_{targ}$ | | | |
| S4 | Cold 1 | 25 | 1000 | 35 | 1010 | 31.5 | 30,692 | |
| S12 | Cold 2 | 0 | 25 | 10 | 35 | 24.0 | 600 | 48.8 |
| S15 | Cold 3 | −44 | 250 | −34 | 260 | 15.3 | 4494 | (Hot Utility) |
| S1 | Cold 4 | 200 | 1000 | 210 | 1010 | 16.3 | 13,013 | |
| S9 | Hot 1 | 1552 | 0 | 1542 | −10 | 42.7 | −66,213 | −72.8 |
| S10 | Hot 2 | 126 | −100 | 116 | −110 | 29.0 | −6555 | (Cold Utility) |

**Table 8.** Heat balances for the temperature intervals in the plasma-assisted dry methane reforming (P-DMR) process.

| Temperature (°C) | Stream Overlapping | ΔT (°C) | $\Delta Cp_{(H,C)}$ (kW/°C) | ΔH (kW) | Surplus/Deficit |
|---|---|---|---|---|---|
| 1542 | 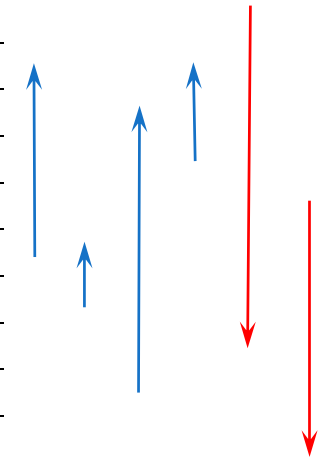 | 532 | −42.7 | −22,697 | Surplus |
| 1010 | | 750 | 5.1 | 3812 | Deficit |
| 260 | | 50 | 20.4 | 1018 | Deficit |
| 210 | | 94 | 4.1 | 386 | Deficit |
| 116 | | 81 | −24.9 | −2017 | Surplus |
| 35 | | 25 | −32.4 | −810 | Surplus |
| 10 | | 20 | −56.4 | −1128 | Surplus |
| −10 | | 24 | −13.7 | −329 | Surplus |
| −34 | | 76 | −29.0 | −2204 | Surplus |
| −110 | | - | - | - | - |
| | C1 C2 C3 C4 H1 H2 | | | | |

**Table 9.** Problem table algorithm for the required utilities in plasma-assisted dry methane reforming (P-DMR) process.

| T (°C) | Hot Utility | ΔH (kW) |
|---|---|---|
| 1542 | ↓ | 0 |
| | ΔH = −22,696.7 kW | |
| 1010 | ↓ | 22,696.7 |
| | ΔH = 3812.2 kW | |
| 260 | ↓ | 18,884.5 |
| | ΔH = 1018.4 kW | |
| 210 | ↓ | 17,866.1 |
| | ΔH = 385.5 kW | |
| 116 | ↓ | 17,480.6 |
| | ΔH = −2017.1 kW | |
| 35 | ↓ | 19,497.7 |
| | ΔH = −809.9 kW | |
| 10 | ↓ | 20,307.6 |
| | ΔH = −1127.6 kW | |
| -10 | ↓ | 21,435.2 |
| | ΔH = −329.2 kW | |
| -34 | ↓ | 21,764.5 |
| | ΔH = −2204.2 kW | |
| -110 | ↓ | 23,968.7 |
| | **Cold utility** | |

The heat exchanger network of the plasma-assisted DMR process is presented in Figure 14. Five process-to-process streams heat exchangers and two coolers are required for the heat integration. The

cold streams are heated up to the target temperature without extra hot utility. The two extra coolers cool the hot streams down to the target temperature.

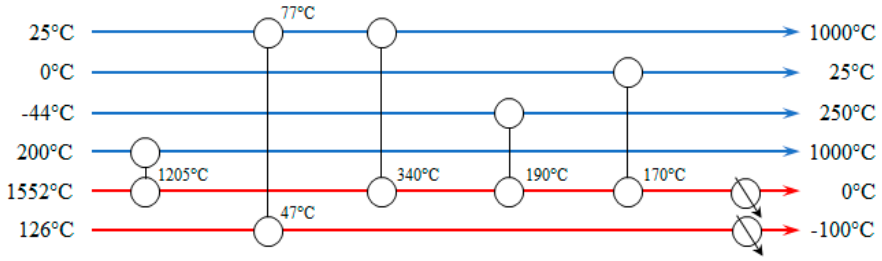


**Figure 14.** Heat exchanger network for the plasma-assisted dry methane reforming (P-DMR) process.

Both processes manage to reduce the utilities demand after the heat integration. In Table 10, the hot and cold utility demand before and after heat integration is presented; 95.4% and 79.7% less hot and cold utility, respectively, is required in thermal catalytic DMR; no hot utility and reduced cold utility by 67% is required in the plasma-assisted DMR process. The utility demand reduction is attained at the expense of capital investment. The number of heat exchangers increases, thus capital investment increases too. However, the objective is to attain highly energy efficient DMR processes and the heat exchangers cost is not expected to significantly raise the capital investment.

**Table 10.** Hot and cold utility demand before and after heat integration.

| DMR Processes | Hot Utility, MW | | Cold Utility, MW | |
|---|---|---|---|---|
| | Before Heat Integration | After Heat Integration | Before Heat Integration | After Heat Integration |
| Thermal catalytic DMR process | 45.7 | 2.1 | 56.7 | 11.0 |
| Plasma-assisted DMR process | 48.8 | - | 72.8 | 24 |

### *2.5. Equipment Cost Estimation*

The cost of the process equipment needed for syngas production through thermal catalytic and plasma-assisted DMR is estimated. The equipment cost is estimated using cost equations, which are based on the key characteristic of each piece of equipment [71]. The key characteristic of each piece of equipment is obtained from the process simulation.

The cost of thermal catalytic DMR, SMR, WGS and SCMR reactors is estimated by the following equation:

$$C = 1.218 \times k \times (1 + f_d + f_p) \times Q^{0.86} \quad (11)$$

The reactors are fired heaters, box type reformers, made of carbon steel and operating at moderate pressure. The key characteristic of the thermal catalytic reactors is the net heat duty.

The cost of compressors is estimated by the following equation:

$$C = 7.19 \times (HP)^{0.61} \quad (12)$$

Reciprocating compressors are used for the gas transportation and compression. The key characteristic of the compressors is the indicated horsepower required for gas transportation and compression to the target pressure.

Shell-and-tube heat exchangers made of carbon steel are employed to build the heat exchanger network. The key characteristic is the heat exchange area and the cost is estimated by the equation:

$$C = 1.218 \times f_d \times f_m \times f_p \times C_b \quad (13)$$

where $C_b = \exp\left[8.821 - 0.30863 \times \ln A + 0.0681 \times (\ln A)^2\right]$ ;

$f_d = \exp\left[-1.1156 + 0.0906 \times \ln A\right]$; $f_m = 1$; $f_p = 1$ .

The cost of coolers which operate at 20 °C is given by the same equation as the heat exchangers cost. The cost of the coolers, which operate at lower temperature (0 °C, −10 °C and −100 °C), is given by:

$$C = 178 \times F \times Q^{0.61} \quad (14)$$

where F is 1, 1.55 and 4 for 0 °C, −10 °C and −100 °C, respectively.

The cost of the plasma reactor is based on the lab scale plasma reactor cost, which was used by Scapinello et al. [31] and reached ~8 k$. The cost also takes into account the cost of repetitive nanosecond pulsed power unit and the six-tenth power rule is used to estimate the installed cost of the plasma reactor at industrial scale. Eventually, using installation factors, the purchase equipment costs are converted into installed costs. The purchase and installed process equipment cost for thermal catalytic and plasma-assisted DMR process are presented in Tables 11 and 12 respectively. Regarding the thermal catalytic process, compressors have the highest contribution to the equipment cost. SMR and DMR reactors are also significant costs. In the plasma-assisted process, the plasma reactor is the most expensive piece of equipment. Compressors and refrigeration systems are also expensive equipment units.

**Table 11.** Total equipment cost of the thermal catalytic DMR process.

| Thermal Catalytic DMR Process | | | |
|---|---|---|---|
| **Equipment** | **Purchase Cost, M$** | **Installation Factor** | **Installed Cost, M$** |
| DMR | - | - | 1.522 |
| SMR | - | - | 3.056 |
| WGS | - | - | 0.132 |
| Comp1 | 2.376 | 1.3 | 3.089 |
| Comp2 | 0.806 | 1.3 | 1.047 |
| Comp3 | 0.589 | 1.3 | 0.765 |
| Comp4 | 1.609 | 1.3 | 2.091 |
| Comp5 | 1.266 | 1.3 | 1.645 |
| Comp6 | 0.895 | 1.3 | 1.163 |
| HX-1 | 0.004 | 2.0 | 0.008 |
| HX-2 | 0.020 | 2.0 | 0.040 |
| HX-3 | 0.013 | 2.0 | 0.027 |
| HX-4 | 0.004 | 2.0 | 0.008 |
| HX-5 | 0.003 | 2.0 | 0.006 |
| HX-6 | 0.007 | 2.0 | 0.014 |
| HX-7 | 0.018 | 2.0 | 0.035 |
| HX-8 | 0.005 | 2.0 | 0.009 |
| HX-9 | 0.007 | 2.0 | 0.014 |
| Cooler-1 | 0.049 | 2.0 | 0.098 |
| Cooler-2 | 0.017 | 2.0 | 0.035 |
| Cooler-4 | 0.015 | 2.0 | 0.030 |
| Cooler-5 | 0.012 | 2.0 | 0.024 |
| Cooler-3 (Refrigeration system) | - | - | 0.785 |
| Total equipment cost | | | 15.644 |

**Table 12.** Total equipment cost of the plasma-assisted DMR process.

| Plasma-Assisted DMR Process | | | |
|---|---|---|---|
| **Equipment** | **Purchase Cost, M$** | **Installation Factor** | **Installed Cost, M$** |
| SCMR | - | - | 1.339 |
| P-DMR | - | - | 7.100 |
| Comp1 | 3.658 | 1.3 | 4.755 |
| Comp2 | 0.974 | 1.3 | 1.266 |
| Comp3 | 0.494 | 1.3 | 0.643 |
| HX-1 | 0.014 | 2.0 | 0.028 |
| HX-2 | 0.006 | 2.0 | 0.012 |
| HX-3 | 0.008 | 2.0 | 0.016 |
| HX-4 | 0.010 | 2.0 | 0.021 |
| HX-5 | 0.003 | 2.0 | 0.006 |
| Cooler-1 (Refrigeration system) | - | - | 4.119 |
| Cooler-2 (Refrigeration system) | - | - | 4.490 |
| Total equipment cost | | | 23.795 |

## 3. Comparison of Thermal Catalytic and Plasma-Assisted DMR

Thermal catalytic and plasma-assisted DMR differentiate in many aspects, which makes a fair comparison between the two processes very challenging. The aim of the comparison herein is not to propose the most promising process, but rather to address the strengths and weaknesses of each one. Specific performance criteria have been quantified and presented in Table 13 to this end. The estimated values have been based on the mass and energy balances that have been obtained through the simulations.

**Table 13.** Quantified performance criteria for thermal catalytic and plasma-assisted DMR process.

| **Process** | **Resource Efficiency** $kmol_{syngas}/kmol_i$ | | | **Hot Utility** $kWh/kmol_{syngas}$ | **Electricity** $kWh/kmol_{syngas}$ | **Investment** $k\$/kmol_{syngas}\ h^{-1}$ |
|---|---|---|---|---|---|---|
| - | $CH_4$ | $CO_2$ | $H_2O$ | - | - | - |
| Thermal catalytic DMR | 4.14 | 12.83 | 4.88 | 15.7 | 5.4 | 3.9 |
| Plasma-assisted DMR | 3.69 | 9.15 | 7.90 | - | 37 + 12.7 = 49.7 | 12.9 |

Raw material (resource) is the cost driver of the syngas production process [19]. Thus, resource efficiency constitutes a key criterion of process performance. For each mole of $CH_4$ that is cracked, 12.2% more syngas is produced by the thermal catalytic process due to less coke formation as compared with the plasma-assisted process. For each mole of $CO_2$ cracked, 40.2% more syngas is produced globally in the thermal catalytic DMR. $CO_2$ is not only cracked in DMR reactor but also produced in WGS reactor. However, when the WGS outlet stream is mixed with the syngas produced in the SMR reactor, the stream meets the targeted ratio of $H_2/(2CO + 3CO_2) \geq 1$. All $CO_2$ is going to be consumed in the methanol synthesis process, thus it is considered that $CO_2$ is fully utilized in the thermal catalytic DMR process. In the plasma-assisted DMR, only 42.5% of $CO_2$ is converted per pass and lower amount of syngas is finally formed in the process. From the economic perspective, there is not a considerable impact on process economics since in the latter case, $CO_2$ is reclaimed and reused. Considering that resource efficiency estimation (Table 13) includes only the $CO_2$ amount that has been cracked for syngas production, it is concluded that higher amount of $CO_2$ is consumed in the plasma-assisted process for a kmol of syngas production. From the environmental point of view, plasma-assisted DMR is more sustainable and, thus, favorable since a higher amount of $CO_2$ is depleted. Eventually, for each mole of $H_2O$ consumed in the process, a higher amount of syngas is produced in the plasma-assisted process implying that $H_2O$ saving is higher in the plasma-assisted process.

Expectantly, the electricity demand for the plasma-assisted DMR process is ten times the demand of the thermal catalytic one; the highest portion (approximately 74%) of electricity is consumed in electron impact reactions occurring in the plasma zone. The capital investment for the plasma-assisted DMR process is rather high. Refrigeration systems, compressors and the plasma reactor form the major capital expenditures.

Other aspects that could be counted as crucial performance criteria are the catalyst demand, by-products formation and the process complexity. In thermal catalytic DMR, three different catalysts are used for the DMR, WGS and SMR reactions while in the plasma-assisted process, catalyst is used to enhance only the SCMR reaction. Less catalyst demand may considerably decrease the syngas production cost. In addition, no auxiliary equipment is required for catalyst regeneration. Ethylene, acetylene and ethane are formed as by-products in the plasma zone. Depending on the production rate and the separation cost, these $C_2$ species can potentially be reclaimed and sold, increasing the economic potential of the plasma-assisted DMR process. Further, the electricity required for plasma initiation may be drawn by onshore or offshore electricity production systems.

## 4. Conclusions

Dry methane reforming (DMR) is considered a promising chemical process with high economic and environmental interest. In the conventional DMR process, activation of $CH_4$ and $CO_2$ is promoted by catalysts and relatively high temperature. Alternatively, electricity can be utilized to initiate plasma, which will lead to reactants bond cracking. Undoubtedly, thermal catalytic and plasma-assisted DMR have strengths and downsides. In the current work, plasma-assisted DMR performed by Scapinello et al. [31] resulted in $H_2$/CO molar ratio equal to 1.1, while thermal catalytic DMR performed by Theofanidis et al. [24] resulted in $H_2$/CO = 1. Considering that syngas suitable for methanol synthesis is the targeted product in this work and the molar ratio required by the Fischer–Tropsch process for methanol production is 2/1, the $H_2$/CO ratio should be increased in both cases. However, in plasma-assisted DMR, less intensive downstream processing is required in terms of equipment. Particularly, plasma-assisted DMR integrated with combined steam/carbon dioxide methane reforming (SCMR) is an effective way to produce syngas for methanol, ethanol or ethylene where a $H_2$/CO molar ratio equal to 2 is required. Its performance is comparable with the performance of integrated thermal catalytic DMR and steam methane reforming (SMR), which has also been proposed for $H_2/CO \geq 2$ syngas production.

Higher amount of $CO_2$ (40% more) per mol of produced syngas is consumed in the plasma-assisted DMR process, as compared with the combined DMR and SMR thermal catalytic process. Concurrently, higher amount of $H_2O$ (62% more) per mol of produced syngas is consumed in the latter case. Plasma-assisted DMR is more sustainable than the combined DMR and SMR thermal catalytic process as it increases $CO_2$ capture; it reduces $H_2O$ scarcity by utilizing more efficiently $H_2O$ input streams, and it is compatible with renewable energy technologies from which the electricity needed for the plasma initiation may be harvested.

As a follow up, the plasma-assisted process may be more easily integrated with existing processes since it is relatively more compact than the thermal catalytic one. Moreover, except for electricity, no utilities are required since the cold utility demand is satisfied by the refrigerant, while, in the thermal catalytic processes, cooling water is required. Regarding the electricity demand, plasma reactors may draw the electricity produced by renewable energy systems. In this case, the gains are that no additional power supply systems are required, no $NO_x$ are released and the plasma reactor absorbs the overproduction of electricity picks contributing to grid stabilization. Short start-up/shut-down periods are also counted as unique technology features compared to the thermal catalytic process.

**Supplementary Materials:** The following are available online at www.mdpi.com/1996-1073/10/9/1429/s1. Figure S1: Plasma assisted DMR process simulation: in black, the process streams; and, in blue, the heat exchangers and the refrigeration systems, Table S1: Mass and energy balances for all the streams of plasma assisted DMR process, Figure S2: Thermal catalytic DMR process simulation (combined DMR and SMR): in black, the process streams;

and, in blue, the heat exchangers and the refrigeration systems, Table S2: Mass and energy balances for all the streams of thermal catalytic DMR process

**Acknowledgments:** Funding: this work has received funding from the European Union's Horizon 2020 Research and Innovation Programme through project "Adaptable Reactors for Resource and Energy Efficient Methane Valorization" (ADREM), No. 680777.

**Author Contributions:** The authors have collectively contributed to this worked.

**Conflicts of Interest:** The authors declare no conflict of interest.

**Glossary**

| | |
|---|---|
| FT | Fischer-Tropsch process |
| DMR | Dry methane reforming |
| DBD | Dielectric barrier discharge |
| GTL | Gas to liquid |
| PBD | Process block diagram |
| RGIBBS | Reactor; equilibrium calculations is based on that minimizes Gibbs free energy |
| RWGS | Reversed water gas shift |
| PSA | Pressure swing adsorption |
| SCMR | Combined steam/carbon dioxide methane reforming |
| WGS | Water gas shift |
| CCS | Carbon capture and storage |
| MEA | Monoethanolamine process |
| SMR | Steam methane reforming |
| P-DMR | Plasma-assisted dry methane reforming |
| RSTOIC | Reactor for known reaction stoichiometry |
| PFD | Process flow diagram |
| $\Delta T_{min}$ | Minimum temperature approach |
| $\Delta H$ | Enthalpy |
| GCC | Grand composite curve |
| $CP_M$ | Mass heat capacity |
| C | Equipment cost |
| Q | Heat duty |
| Comp | Compressor |
| HX | Heat exchanger |

## References

1. Jiao, F.; Li, J.; Pan, X.; Xiao, J.; Li, H.; Ma, H.; Wei, M.; Pan, Y.; Zhou, Z.; Li, M.; et al. Selective conversion of syngas to light olefins. *Science* **2016**, *351*, 1065–1068, doi:10.1126/science.aaf1835.
2. Zhu, Y.; Pan, X.; Jiao, F.; Li, J.; Yang, J.; Ding, M.; Han, Y.; Liu, Z.; Bao, X. Role of manganese oxide in syngas conversion to light olefins. *ACS Catal.* **2017**, *7*, 2800–2804, doi:10.1021/acscatal.7b00221.
3. Cheng, K.; Gu, B.; Liu, X.; Kang, J.; Zhang, Q.; Wang, Y. Direct and highly selective conversion of synthesis gas into lower olefins: Design of a bifunctional catalyst combining methanol synthesis and carbon-carbon coupling. *Angew. Chem.* **2016**, *55*, 4725–4728, doi:10.1002/anie.201601208.
4. Kim, T.W.; Kleitz, F.; Jun, J.W.; Chae, H.J.; Kim, C.U. Catalytic conversion of syngas to higher alcohols over mesoporous perovskite catalysts. *J. Ind. Eng. Chem.* **2016**, *51*, 196–205, doi:10.1016/j.jiec.2017.02.032.
5. Wang, Z.; Kumar, N.; Spivey, J.J. Preparation and characterization of lanthanum-promoted cobalt-copper catalysts for the conversion of syngas to higher oxygenates: Formation of cobalt carbide. *J. Catal.* **2016**, *339*, 1–8, doi:10.1016/j.jcat.2016.03.030.
6. Rao, V.U.S.; Stiegel, G.J.; Cinquegrane, G.J.; Srivastava, R.D. Iron-based catalysts for slurry-phase fischer-tropsch process: Technology review. *Fuel Process. Technol.* **1992**, *30*, 83–107, doi:10.1016/0378-3820(92)90077-4.
7. Scapinello, M.; Delikonstantis, E.; Stefanidis, G.D. The panorama of plasma-assisted non-oxidative methane reforming. *Chem. Eng. Process. Process Intensif.* **2016**, *117*, 120–140, doi:10.1016/j.cep.2017.03.024.
8. Lavoie, J. Review on dry reforming of methane, a potentially more environmentally-friendly approach to the increasing natural gas exploitation. *Front. Chem.* **2014**, *2*, 81, doi:10.3389/fchem.2014.00081.

9. Nematollahi, B.; Rezaei, M.; Khajenoori, M. Combined dry reforming and partial oxidation of methane to synthesis gas on noble metal catalysts. *Int. J. Hydrogen Energy* **2011**, *36*, 2969–2978, doi:10.1016/j.ijhydene.2010.12.007.
10. Sadykov, V.A.; Gubanova, E.L.; Sazonova, N.N.; Pokrovskaya, S.A.; Chumakova, N.A.; Mezentseva, N.V.; Bobin, A.S.; Gulyaev, R.V.; Ishchenko, A.V.; Krieger, T.A.; et al. Dry reforming of methane over Pt/PrCeZrO catalyst: Kinetic and mechanistic features by transient studies and their modeling. *Catal. Today* **2011**, *171*, 140–149, doi:10.1016/j.cattod.2011.04.004.
11. Tsyganok, A.I.; Inaba, M.; Tsunoda, T.; Hamakawa, S.; Suzuki, K.; Hayakawa, T. Dry reforming of methane over supported noble metals: A novel approach to preparing catalysts. *Catal. Commun.* **2003**, *4*, 493–498, doi:10.1016/S1566-7367(03)00130-4.
12. Pakhare, D.; Spivey, J. A review of dry ($CO_2$) reforming of methane over noble metal catalysts. *Chem. Soc. Rev.* **2014**, *43*, 7813–7837, doi:10.1039/C3CS60395D.
13. Ashok, J.; Kawi, S. Steam reforming of toluene as a biomass tar model compound over $CeO_2$ promoted Ni/CaOeAl$_2$O$_3$ catalytic systems. *Int. J. Hydrogen Energy* **2013**, *38*, 13938–13949, doi:10.1016/j.ijhydene.2013.08.029.
14. Chirokov, A.; Gutsol, A.; Fridman, A. Atmospheric pressure plasma of dielectric barrier discharges. *Pure Appl. Chem.* **2005**, *77*, 487–495, doi:10.1351/pac200577020487.
15. Khoja, A.H.; Tahir, M.; Aishah, N.; Amin, S. Dry reforming of methane using different dielectric materials and DBD plasma reactor configurations. *Energy Convers. Manag.* **2017**, *144*, 262–274, doi:10.1016/j.enconman.2017.04.057.
16. Chung, W.; Pan, K.; Lee, H.; Chang, M. Dry reforming of methane with dielectric barrier discharge and ferroelectric packed-bed reactors. *Energy Fuels* **2014**, *28*, 7621–7631, doi:10.1021/ef5020555.
17. Wang, Q.; Yan, B.-H.; Jin, Y.; Cheng, Y. Investigation of dry reforming of methane in a dielectric barrier discharge reactor. *Plasma Chem. Plasma Process.* **2009**, *29*, 217–228, doi:10.1007/s11090-009-9173-3.
18. Iza, F.; Walsh, J.L.; Kong, M.G. From submicrosecond- to nanosecond-pulsed atmospheric-pressure plasmas. *IEEE Trans. Plasma Sci.* **2009**, *37*, 1289–1296, doi:10.1109/TPS.2009.2014766.
19. Zhang, C.; Jun, K.W.; Gao, R.; Lee, Y.J.; Kang, S.C. Efficient utilization of carbon dioxide in gas-to-liquids process: Process simulation and techno-economic analysis. *Fuel* **2015**, *157*, 285–291, doi:10.1016/j.fuel.2015.04.051.
20. Iglesia, E.; Spivey, J.; Fleisch, T. Studies in Surface Science and Catalysis. In Proceedings of the 6th Natural Gas Conversion Symposium, Girdwood, AK, USA, 17–22 June 2011; Elsevier Science B.V.: Amsterdam, The Netherlands, 2001.
21. Gusev, A.V.; Kornev, R.A.; Sukhanov, A.Y. Behavior of carbon-containing impurities during plasma synthesis of trichlorosilane. *High Energy Chem.* **2008**, *42*, 56–58, doi:10.1007/s10733-008-1011-2.
22. Kabadi, V.N.; Danner, R.P. Modified soave-redlich-kwong equation of state for water-hydrocarbon phase equilibria. *Ind. Eng. Chem. Process Des. Dev.* **1985**, *24*, 537–541, doi:10.1021/i200030a004.
23. Tao, X.; Bai, M.; Li, X.; Long, H.; Shang, S.; Yin, Y.; Dai, X. $CH_4$-$CO_2$ reforming by plasma—Challenges and opportunities. *Prog. Energy Combust. Sci.* **2011**, *37*, 113–124, doi:10.1016/j.pecs.2010.05.001.
24. Theofanidis, S.A.; Galvita, V.V.; Poelman, H.; Marin, G.B. Enhanced carbon-resistant dry reforming Fe-Ni catalyst: Role of Fe. *ACS Catal.* **2015**, *5*, 3028–3039, doi:10.1021/acscatal.5b00357.
25. Hla, S.S.; Park, D.; Duffy, G.J.; Edwards, J.H.; Roberts, D.G.; Ilyushechkin, A.; Morpeth, L.D.; Nguyen, T. Kinetics of high-temperature water-gas shift reaction over two iron-based commercial catalysts using simulated coal-derived syngases. *Chem. Eng. J.* **2009**, *146*, 148–154, doi:10.1016/j.cej.2008.09.023.
26. Zhu, M.; Wachs, I.E. Iron-Based Catalysts for the high-temperature water-gas shift (HT-WGS) reaction: A review. *ACS Catal.* **2016**, *6*, 722–732, doi:10.1021/acscatal.5b02594.
27. Bobrova, I.I.; Bobrov, N.N.; Chesnokov, V.V.; Parmon, V.N. Catalytic steam reforming of methane: New data on the contribution of homogeneous radical reactions in the gas phase: II. A ruthenium catalyst. *Kinet. Catal.* **2001**, *42*, 805–812, doi:10.1023/A:1013283216707.
28. Wu, H.; la Parola, V.; Pantaleo, G.; Puleo, F.; Venezia, A.; Liotta, L. Ni-based catalysts for low temperature methane steam reforming: Recent results on Ni-Au and comparison with other Bi-metallic systems. *Catalysts* **2013**, *3*, 563–583, doi:10.3390/catal3020563.
29. Muller, C.R.; Pacciani, R.; Bohn, C.D.; Scott, S.A.; Dennis, J.S. Investigation of the enhanced water gas shift reaction using natural and synthetic sorbents for the capture of $CO_2$. *Ind. Eng. Chem. Res.* **2009**, *48*, 10284–10291, doi:10.1021/Ie900772q.

30. Jang, W.; Jeong, D.; Shim, J.-O.; Kim, H.; Roh, H.; Son, I.H.; Lee, S.J. Combined steam and carbon dioxide reforming of methane and side reactions: Thermodynamic equilibrium analysis and experimental application. *Appl. Energy* **2016**, *173*, 80–91, doi:10.1016/j.apenergy.2016.04.006.
31. Scapinello, M.; Martini, L.M.; Dilecce, G.; Tosi, P. Conversion of $CH_4/CO_2$ by a nanosecond repetitively pulsed discharge. *J. Phys. D Appl. Phys.* **2016**, *49*, 75602, doi:10.1088/0022-3727/49/7/075602.
32. Damyanova, S.; Pawelec, B.; Arishtirova, K.; Fierro, J.L.G. Ni-based catalysts for reforming of methane with $CO_2$. *Int. J. Hydrogen Energy* **2012**, *37*, 15966–15975, doi:10.1016/j.ijhydene.2012.08.056.
33. Golmakani, A.; Fatemi, S.; Tamnanloo, J. Investigating PSA, VSA, and (TSA) methods in (SMR) unit of refineries for hydrogen production with fuel cell specification. *Sep. Purif. Technol.* **2017**, *176*, 73–91, doi:10.1016/j.seppur.2016.11.030.
34. Chowdhury, D.R.; Sarkar, S.C. Application of pressure swing adsorption cycle in the quest of production of oxygen and nitrogen. *Int. J. Eng. Sci. Innov. Technol.* **2016**, *5*, 64–69.
35. Hamilton, H. Palladium-based membranes for hydrogen separation. *Platin. Met. Rev.* **2012**, *56*, 117–123, doi:10.1595/147106712X632460.
36. Olah, G.A.; Prakash, G.K.S.; Goeppert, A. Anthropogenic chemical carbon cycle for a sustainable future. *J. Am. Chem. Soc.* **2011**, *133*, 12881–12898, doi:10.1021/ja202642y.
37. Olah, G.A.; Goeppert, A.; Czaun, M.; Prakash, G.K.S. Bi-reforming of methane from any source with steam and carbon dioxide exclusively to metgas (CO-2$H_2$) for methanol and hydrocarbon synthesis. *J. Am. Chem. Soc.* **2013**, *135*, 648–650, doi:10.1021/ja311796n.
38. Santos, B.A.V.; Loureiro, J.M.; Ribeiro, A.M.; Rodrigues, A.E.; Cunha, A.F. Methanol production by bi-reforming. *Can. J. Chem. Eng.* **2015**, *93*, 510–526, doi:10.1002/cjce.22068.
39. Herguido, J.; Corella, J.; Gonzalez-Saiz, J. Steam gasification of lignocellulosic residues in a fluidized bed at a small pilot scale. Effect of the type of feedstock. *Ind. Eng. Chem. Res.* **1992**, *31*, 1274–1282, doi:10.1021/ie00005a006.
40. Khan, Z.; Inayat, A.; Yusup, S.; Ahmad, M.M. Kinetic parameters determination using optimization approach in integrated catalytic adsorption steam gasification for hydrogen production. *Int. J. Hydrogen Energy* **2015**, *40*, 8824–8832, doi:10.1016/j.ijhydene.2015.05.069.
41. Twigg, M.V. *Catalyst Handbook*, 2nd ed.; Manson: London, UK, 1996.
42. Jockenhoevel, T.; Schneider, R.; Rode, H. Development of an economic post-combustion carbon capture process. *Energy Procedia* **2009**, *1*, 1043–1050, doi:10.1016/j.egypro.2009.01.138.
43. Yan, S.; Fang, M.; Zhang, W.; Zhong, W.; Luo, Z.; Cen, K. Comparative analysis of $CO_2$ separation from flue gas by membrane gas absorption technology and chemical absorption technology in China. *Energy Convers. Manag.* **2008**, *49*, 3188–3197, doi:10.1016/j.enconman.2008.05.027.
44. Sayari, A.; Belmabkhout, Y.; Serna-Guerrero, R. Flue gas treatment via $CO_2$ adsorption. *Chem. Eng. J.* **2011**, *171*, 760–774, doi:10.1016/j.cej.2011.02.007.
45. Sjostrom, S.; Krutka, H. Evaluation of solid sorbents as a retrofit technology for $CO_2$ capture. *Fuel* **2010**, *89*, 1298–1306, doi:10.1016/j.fuel.2009.11.019.
46. Mavroudi, M.; Kaldis, S.P.; Sakellaropoulos, G.P. Reduction of $CO_2$ emissions by a membrane contacting process. *Fuel* **2003**, *82*, 2153–2159, doi:10.1016/S0016-2361(03)00154-6.
47. Xu, G.; Liang, F.; Yang, Y.; Hu, Y.; Zhang, K.; Liu, W. An improved $CO_2$ separation and purification system based on cryogenic separation and distillation theory. *Energies* **2014**, *7*, 3484–3502, doi:10.3390/en7053484.
48. Besong, M.T.; Maroto-Valer, M.M.; Finn, A.J. Study of design parameters affecting the performance of $CO_2$ purification units in oxy-fuel combustion. *Int. J. Greenh. Gas Control* **2013**, *12*, 441–449, doi:10.1016/j.ijggc.2012.11.016.
49. Jana, A.K. Heat integrated distillation operation. *Appl. Energy* **2010**, *87*, 1477–1494, doi:10.1016/j.apenergy.2009.10.014.
50. Luis, P. Use of monoethanolamine (MEA) for $CO_2$ capture in a global scenario: Consequences and alternatives. *Desalination* **2016**, *380*, 93–99, doi:10.1016/j.desal.2015.08.004.
51. Luyben, W.L. Design and control of the dry methane reforming process. *Ind. Eng. Chem. Res.* **2014**, *53*, 14423–14439, doi:10.1021/ie5023942.
52. Alie, C.; Backham, L.; Croiset, E.; Douglas, P.L. Simulation of $CO_2$ capture using MEA scrubbing: A flowsheet decomposition method. *Energy Convers. Manag.* **2005**, *46*, 475–487, doi:10.1016/j.enconman.2004.03.003.

53. Jung, J.; Jeong, Y.S.; Lim, Y.; Lee, C.S.; Han, C. Advanced $CO_2$ capture process using MEA scrubbing: Configuration of a split flow and phase separation heat exchanger. *Energy Procedia* **2013**, *37*, 1778–1784, doi:10.1016/j.egypro.2013.06.054.
54. Singh, D.; Croiset, E.; Douglas, P.L.; Douglas, M.A. Techno-economic study of $CO_2$ capture from an existing coal-fired power plant: MEA scrubbing vs. $O_2/CO_2$ recycle combustion. *Energy Convers. Manag.* **2003**, *44*, 3073–3091, doi:10.1016/S0196-8904(03)00040-2.
55. Xu, G.; Li, L.; Yang, Y.; Tian, L.; Liu, T.; Zhang, K. A novel CO2 cryogenic liquefaction and separation system. *Energy* **2012**, *42*, 522–529, doi:10.1016/j.energy.2012.02.048.
56. Soave, G.S.; Gamba, S.; Pellegrini, L.A.; Bonomi, S. Feed-splitting technique in cryogenic distillation. *Ind. Eng. Chem. Res.* **2006**, *45*, 5761–5765, doi:10.1021/ie051343e.
57. Salerno, D.; Arellano-Garcia, H.; Wozny, G. Ethylene separation by feed-splitting from light gases. *Energy* **2011**, *36*, 4518–4523, doi:10.1016/j.energy.2011.03.064.
58. Li, X.; Li, J.; Yang, B. Design and control of the cryogenic distillation process for puri fi cation of synthetic natural gas from methanation of coke oven gas. *Ind. Eng. Chem. Res.* **2014**, *53*, 19583–19593.
59. Ryi, S.K.; Lee, S.W.; Park, J.W.; Oh, D.K.; Park, J.S.; Kim, S.S. Combined steam and $CO_2$ reforming of methane using catalytic nickel membrane for gas to liquid (GTL) process. *Catal. Today* **2014**, *236*, 49–56, doi:10.1016/j.cattod.2013.11.001.
60. Danilova, M.M.; Fedorova, Z.A.; Kuzmin, V.A.; Zaikovskii, V.I.; Porsin, A.V.; Krieger, T. Combined steam and carbon dioxide reforming of methane over porous nickel based catalysts. *Catal. Sci. Technol.* **2015**, *5*, 2761–2768, doi:10.1039/C4CY01614A.
61. Gangadharan, P.; Kanchi, K.C.; Lou, H.H. Evaluation of the economic and environmental impact of combining dry reforming with steam reforming of methane. *Chem. Eng. Res. Des.* **2012**, *90*, 1956–1968, doi:10.1016/j.cherd.2012.04.008.
62. Basini, L.; Piovesan, L. Reduction on synthesis gas costs by decrease of steam/carbon and oxygen/carbon ratios in the feedstock. *Ind. Eng. Chem. Res.* **1998**, *37*, 258–266, doi:10.1021/ie970402o.
63. Brunet, R.; Boer, D.; Guillén-Gosálbez, G.; Jiménez, L. Reducing the cost, environmental impact and energy consumption of biofuel processes through heat integration. *Chem. Eng. Res. Des.* **2015**, *93*, 203–212, doi:10.1016/j.cherd.2014.06.018.
64. Zhang, C.; Jun, K.W.; Gao, R.; Kwak, G.; Park, H.G. Carbon dioxide utilization in a gas-to-methanol process combined with $CO_2$/steam-mixed reforming: Techno-economic analysis. *Fuel* **2017**, *190*, 303–311, doi:10.1016/j.fuel.2016.11.008.
65. Zhang, X.; Cha, M.S. Electron-induced dry reforming of methane in a temperature-controlled dielectric barrier discharge reactor. *J. Phys. D. Appl. Phys.* **2013**, *46*, 415205, doi:10.1088/0022-3727/46/41/415205.
66. Kogelschatz, U. Dielectric-barrier discharges: Their history, discharge physics, and industrial applications. *Plasma Chem. Plasma Process.* **2003**, *23*, 1–46, doi:10.1023/A:1022470901385.
67. Penteado, A.; Esche, E.; Salerno, D.; Godini, H.R.; Wozny, G. Design and assessment of a membrane and absorption based carbon dioxide removal process for oxidative coupling of methane. *Ind. Eng. Chem. Res.* **2016**, *55*, 7473–7483, doi:10.1021/acs.iecr.5b04910.
68. Whyte, T.E.; Yon, C.M.; Wagener, E.H. *Industrial Gas Separations*; ACS Symposium Series 223; American Chemical Society: Washington, DC, USA, 1983.
69. Peng, L.; Park, Y.H.; Moon, D.J.; Park, N.C.; Kim, Y.C. Carbon deposition onto Ni-Based catalysts for combined steam/$CO_2$ reforming of methane. *J. Nanosci. Nanotechnol.* **2016**, *16*, 1562–1566.
70. Kim, A.R.; Lee, H.Y.; Lee, D.H.; Kim, B.W.; Chung, C.H.; Moon, D.J.; Jang, E.J.; Pang, C.; Bae, J.W. Combined steam and $CO_2$ reforming of $CH_4$ on LaSrNiOx mixed oxides supported on $Al_2O_3$-modified SiC support. *Energy Fuels* **2015**, *29*, 1055–1065, doi:10.1021/ef501938v.
71. Couper, J.R.; Penney, R.W.; Fair, J.R.; Walas, S.M. *Chemical Process Equipment: Selection and Design*, 3rd ed.; Butterwoth-Heinemann: Oxford, UK, 2012.